A new plant-specific syntaxin-6 protein may define an intracytoplasmic route for begomoviruses

Bianca Castro Gouveia-Mageste[1&], Laura Gonçalves Costa Martins[1&], Maximiller Dal-Bianco[1,2], João Paulo Batista Machado[1,3], José Cleydson Ferreira da Silva[1], Anésia Aparecida dos Santos[1,4], Joseph R Ecker[5] and Elizabeth Pacheco Batista Fontes[1,2*]

[1]National Institute of Science and Technology in Plant-Pest Interactions, Bioagro, Universidade Federal de Viçosa, Viçosa, Minas Gerais, Brazil

[2]Departament of Biochemistry and Molecular Biology, Universidade Federal de Viçosa, Viçosa, Minas Gerais 36570-000, Brazil

[3]Agronomy Institute, Universidade Federal de Viçosa, Campus Florestal, Florestal, Minas Gerais, Brazil

[4]Departament of General Biology, Universidade Federal de Viçosa, Viçosa, Minas Gerais, Brazil

[5]Howard Hughes Medical Institute and Plant Biology Laboratory, The Salk Institute of Biological Studies, La Jolla, United States of America

*Corresponding author

Email: bbfontes@ufv.br

[&]These authors contributed equally to this work

Running title: NISP in begomovirus intracellular transport

Abstract

Due to limited free diffusion in the cytoplasm, viruses must use active transport mechanisms to move intracellularly. Nevertheless, how the plant ssDNA begomovirus hijacks the host intracytoplasmic transport machinery to move from the nucleus to the plasmodesma remains enigmatic. Here, we identified nuclear shuttle protein (NSP)-interacting proteins by probing a protein microarray and demonstrated that viral NSP, a facilitator of the nucleocytoplasmic trafficking of viral (v)DNA, interacts with a new endosomal vesicle-localized plant-specific syntaxin-6 protein, designated NISP *in planta*. We also showed that begomovirus infection requires the NISP-NSP interaction; NISP displays a pro-viral function, but not the syntaxin-6 paralog AT2G18860 that failed to interact with NSP. Consistent with these findings, *nisp-1* mutant plants were less susceptible to begomovirus infection, a phenotype reversed by NISP complementation, whereas overexpressing lines accumulated higher levels of viral DNA than wild-type. Furthermore, NISP interacts with NIG, another pro-viral factor that accessorizes the NSP-vDNA nucleocytoplasmic translocation. Additionally, the NISP-NIG interaction is enhanced by NSP. We also showed that NISP associates with vDNA and might assemble a NISP-NIG-NSP-vDNA- complex. NISP may function as a docking site for recruiting NIG and NSP into trafficking vesicles, providing a mechanism for the intracytoplasmic translocation of the NSP-vDNA complex towards the cell periphery.

Author Summary

As viruses must use an active and directed intracellular movement, they hijack the intracellular host transport system for their benefit. Therefore, the identification of interactions between host

47 proteins and begomovirus movement proteins should target the intracellular transport machinery.
48 This work focused on the identification of these protein-protein interactions; it addressed the
49 molecular bases for the intracellular transport of begomoviruses. We used a protein microarray to
50 identify cellular partners for the movement protein (MP) and the viral nuclear shuttle protein
51 (NSP), which is a facilitator of the nucleocytoplasmic trafficking of viral (v)DNA. We identified
52 relevant protein-protein interaction (PPI) hubs connecting host and viral proteins. We revealed a
53 novel NSP-interacting protein, which functions in the intracytoplasmic transport of proteins and
54 DNA from begomoviruses and was designated NSP-interacting syntaxin domain-containing
55 protein (NISP). Our data suggest an intracellular route connecting the release of newly-synthesized
56 begomoviral DNA in the cytosol with the cell surface. Resolving viral DNA-host protein
57 complexes led to the identification of a novel class of components of the cell machinery and a
58 representative member, NISP, that functions as a susceptibility gene against begomoviruses. As
59 geminiviruses pose a severe threat to agriculture and food security, this recessive gene can now be
60 exploited as a target for engineering resistance by gene editing in crops.
61
62

63 ## Introduction

64

65 As obligate intracellular parasites, viruses must enter the host cells and hijack the cell
66 machinery to complete their life cycle. Independent on the molecular mechanisms for virus entry
67 into cells, which differ entirely between animal and plant viruses, once in the cytoplasm, both plant
68 and animal viral genomes move intracellularly to specific cellular sub-compartments for
69 replication, transcription or encapsidation [1,2]. Due to the limitation of free diffusion in the
70 cytoplasm, viruses have invoked the endogenous host movement mechanisms for an active and
71 directed intracytoplasmic translocation. In fact, almost all viruses are capable of subverting the
72 microtubule transport system to some extent to replicate and spread. Plant viruses must also use
73 an active mechanism to move the viral genome from the replication site to the plasmodesmata,
74 which are intercellular cytoplasmic bridges between plant cells [2,3]. To promote this typical cell-
75 to-cell movement, plant viruses have evolved movement proteins that increase the size exclusion
76 limit of the plasmodesmata and actively promote the viral nucleic acid translocation into
77 uninfected, adjacent cells [4]. In the case of viruses that replicate in the nuclei of infected cells,
78 they have to be directed to the nuclear periphery, followed by nuclear entry. Likewise, the newly-
79 synthesized viral proteins and viral genomes must translocate throughout the cytoplasm during
80 exit. In animal cells, the retroviruses and DNA viruses deploy the microtubule motor system and
81 microtubule cytoskeleton to move viral proteins and genomes into the nucleus and back to the
82 plasma membrane [1, 5]. Geminiviruses are typical examples of plant DNA viruses that replicate
83 in the nuclei of infected cells, but the underlying mechanisms for the intracytoplasmic movement
84 of viral proteins and viral DNA (vDNA) are far less understood.

85 Geminiviruses are circular single-stranded (ss) DNA viruses, which replicate via double-

86 stranded (ds) DNA intermediates in the nucleus of infected cells, infect a broad spectrum of
87 economically important crops and cause significant yield losses worldwide [6]. The *Geminiviridae*
88 family includes nine genera, but approximately 75% of the identified species belong to the genus
89 *Begomovirus*, which are whitefly-transmitted, infect dicotyledonous species, and display a genome
90 configuration that can be either monopartite or bipartite [7,8]. The genomic components of the
91 bipartite begomoviruses are designated DNA-A and DNA-B. The DNA-A encodes proteins
92 required for viral replication (AC1 or Rep, REn or AC3), transactivation of viral genes (AC2 or
93 TRaP), encapsidation of viral genome (AV1 or CP) and suppression of host defenses (AC4 and
94 TrAP). DNA-B encodes the nuclear shuttle protein (NSP or BV1) and the movement protein (MP
95 or BC1) involved in intracellular and cell-to-cell movement of vDNA.

96 Although the role of MP-NSP complex formation in mediating intracellular and
97 intercellular transport of begomoviruses is widely accepted, the molecular mechanisms underlying
98 the action of these viral proteins at individual stages of the intracellular and intercellular movement
99 are still debated. Some studies indicated that NSP from *Bean dwarf mosaic virus* (BDMV) and
100 *Abutilon mosaic virus* (AbMV) complexes with ss-vDNA and ds-vDNA presumably in the nuclei
101 of infected cells, whereas NSP from *Squash leaf curl virus* (SLCV) binds only ss-vDNA *in vitro*
102 [9, 10, 11]. NSP also interacts with MP in the cytoplasm [12], which promotes the directionality
103 of virus translocation to the cell surface [12, 13]. The mechanism for vDNA exit from the nucleus
104 remains unsolved. It has been conceptually accepted that NSP facilitates the nuclear exit of newly-
105 replicated vDNA via nuclear pores [10, 14-17]. However, the interactions with the host nuclear
106 transport machinery have not been documented. A piece of this puzzle was obtained with the
107 identification of an NSP-interacting GTPase (NIG), which interacts with NSP at the cytosolic side
108 of the nuclear pore complex and facilitates the release of NSP-vDNA complex from the nuclear

109 envelope into the cytosol [12, 18] . Consistent with this transport function, the cytosolic NIG (i)
110 accumulates around the nuclear envelope, (ii) promotes the translocation of NSP-vDNA from the
111 nucleus to the cytoplasm, (iii) functions as a pro-viral factor during begomovirus infection and (iv)
112 shares structural features and transport properties with the human Rev-Interacting Protein (hRIP),
113 which has been shown to be involved in the release of HIV-1 RNAs from the nuclear periphery to
114 the cytoplasm [12, 18, 19]. Histone H3 has been shown to bind NSP and MP from BDMV as an
115 additional component of the vDNA-protein complex that traffics intracellularly and intercellularly
116 [20]. A nuclear acetyltransferase (AtNSI) also interacts with the *Cabbage leaf curl virus*
117 (CaLCuV) NSP and may regulate the nuclear export of ss-vDNA-NSP via acetylation of CP and
118 histones [21, 22]. Other NSP-interacting partners include the receptor-like kinases (RLKs) NSP-
119 interacting kinase (NIK1) and NSP-associated kinase (NsAK), which are not involved in
120 intracellular movement of vDNA but rather are implicated in antiviral immunity against
121 begomoviruses [23-26].

122 For the cell-to-cell transport of vDNA, two distinct mechanisms, which basically differ in
123 the nature of the vDNA-protein complex translocated into adjacent cells, have been suggested [11,
124 27]. In the first mechanism, designated "relay race" model, NSP facilitates the translocation of
125 viral DNA from the nucleus to the cytoplasm and then is replaced by MP, which promotes the cell-
126 to-cell movement of vDNA via plasmodesmata [10, 14]. The second mechanism represented by
127 the "couple-skating" model preconizes that MP facilitates the vDNA-NSP nucleocytoplasmic
128 trafficking and promotes the translocation of vDNA-NSP complex into the adjacent cells via
129 endoplasmic-reticulum-derived tubules induced by the viral infection [11-13, 18, 28-32]. More
130 recently, an alternative route for intracellular translocation and cell-to-cell spread of vDNA via
131 chloroplasts and stromules has been proposed, which was based on experimental data of AbMV

132 MP interactions (33,34). AbMV infection has been shown to induce the formation of a stromule
133 network interconnecting different chloroplasts, chloroplasts with nuclei, and expanding to the cell
134 periphery presumably at plasmodesmata [34]. This stromule network is stabilized by the plastid
135 chaperone cpHSC70, which has also been shown to interact with MP [33]. The interaction between
136 MP and cpHSC70 may bridge viral nucleoprotein complexes with stromules. Independent on the
137 cell-to-cell transport models, the underlying mechanisms of the intracytoplasmic retrograde and
138 anterograde movement of vDNA complexes remain to be determined. CaLCuV and SLCV MPs
139 have been shown to interact with synaptotagmin A (SYTA), which is located in the endosomes of
140 plant cells and is required for the cell-to-cell trafficking of different MPs [35]. These findings
141 raised the hypothesis that distinct viral MPs promote an intracytoplasmic transport of vDNA-
142 complexes to plasmodesmata via an endocytic recycling pathway. Likewise, the AbMV MP has
143 been shown to interfere with microtubule assembly and stability when co-expressed in plant tissues
144 with a viral inducer of cell progression, which may suggest a microtubule-associated transit of MP
145 or begomoviruses to the plasmodesmata [36]. However, the host components of the vDNA
146 complex competent for intracytoplasmic translocation have not been identified, and the underlying
147 mechanism for intracytoplasmic trafficking of vDNA remains to be elucidated.

148 In this investigation, we used a protein microarray assay to identify MP- and NSP-host
149 protein-protein interactions (PPIs). From the NSP-MP-host PPI network map, we selected an
150 intracellular transport-associated protein, designated NSP-interacting syntaxin domain-containing
151 protein (NISP), as an NSP specific target, to gain further insight into the intracytoplasmic transport
152 of begomoviruses. We showed that NISP, which was located in motile vesicle-like structures,
153 many of which were targeted to the endosomes, interacted with NSP *in vivo* and displayed a pro-
154 viral function. Furthermore, NISP also interacted with NIG, and the complex formed was enhanced

155 by the presence of viral NSP. In addition, vDNA was recruited into the NISP complex. Our data
156 indicate that NISP may be part of the vDNA complex that traffics intracellularly via endosomes.
157
158
159 ## Results
160
161 **Identification of Arabidopsis proteins interacting with in vitro transcribed and translated**
162 **MP and NSP**
163 To search for the begomovirus movement proteins-Arabidopsis protein-protein
164 interactions (PPIs), we used a nucleic acid programmable protein array (NAPPA)-based approach
165 [37], in which we interrogated 4600 *in vitro* synthesized ORFs from Arabidopsis for their capacity
166 to be targeted by MP and/or NSP from CaLCuV. The *in situ* synthesized NAPPA protein
167 microarray has previously generated a transcription factor (TF)-NAPPA dataset, which has been
168 validated by pull-down assays and bimolecular fluorescence complementation (BiFC) assays in
169 tobacco leaves using a subset of newly identified interactions [37]. NSP and MP were *in vitro*
170 transcribed and translated to probe this protein microarray (S1a and S1b Fig). A total of 40 proteins
171 were identified as associated with MP, and 40 interacted with NSP. The majority (35 proteins of
172 40) were found to interact with both proteins, which was not surprising because MP itself interacts
173 with NSP and may be part of common multiprotein complexes as both participate in viral DNA
174 movement (S2 Fig). We found five new NSP-specific protein interactions (dark orange) and five
175 MP-specific protein interactions (light yellow), including the stomatal cytokinesis defective 2
176 (SCD2) protein (AT3G48860) and a peptidyl-prolyl cis-trans isomerase family protein
177 (AT1G73655) belonging to the same protein family as Pin4, which have been shown previously

178 to interact with MP (S1 Table) [36]. As previously identified NSP-interacting proteins were absent
179 in the protein array, the identification of known MP-specific interacting proteins contributed to
180 validate our current data.

181 The protein-protein interactions between the viral proteins and the Arabidopsis proteins
182 were integrated into the protein-protein interactome experimentally determined for *Arabidopsis*
183 *thaliana* (BioGRID database and the Arabidopsis interactome database), using Cytoscape
184 software. This procedure identified the PPI network containing MP, NSP and all, directly and
185 indirectly, interacting host proteins (Fig 1). AT1G68185, an ubiquitin-like protein, which formed
186 a large hub (hub 20, degree 148), may represent a convergent targeting node among begomovirus
187 viral proteins as it was found to be a direct target of NSP and MP independently (S1 Table).
188 Furthermore, the ubiquitin-proteasome pathway (UPS) is targeted by many viruses to maintain
189 suitable levels of viral proteins and to induce, inhibit or modify ubiquitin (Ub)-related host proteins
190 [38]. Other MP-interacting proteins, including FKBP-like peptidyl-prolyl cis-trans isomerase
191 family protein (this work), chloroplast heat shock protein 70-1 [33] and synaptotagmin A [35],
192 which have been shown to assist the MP movement function, are connected to the AT1G68185
193 hub (hub 20), further supporting the notion that this hub may be biologically significant during
194 begomovirus infection.

195 To gain further insights into the cellular processes affected by NSP or MP, we performed
196 functional enrichment analyses of their direct and indirect interactors. Significantly enriched GO
197 terms (with p-value < 0.05) were identified in all three categories, Biological Process, Molecular
198 Function, or Cellular Component ontology (S2 Table). Some over-represented GO terms in this
199 set of viral protein-interacting host proteins are consistent with NSP and MP function or
200 localization. Consistent with their function as viral movement proteins, a subset of host interactors

201 was significantly over-represented under the transport activity term and protein binding term in
202 Molecular Function (S2 Table). Under the cellular component ontology, we observed an over-
203 representation of proteins under membrane-bounded organelle term, intracellular vesicle term, and
204 SNARE complex term, which may suggest an intracytoplasmic route for begomovirus proteins
205 and vDNA trafficking (S2 Table). Accordingly, two NSP-interacting proteins, AT5G23550 and
206 AT4G30240, form convergent hubs (17 and 19) enriched for membrane-bound proteins and
207 transport activity function (Fig 1, S1 Table). The NSP-interacting protein AT5G23550 (hub 17)
208 is annotated as a Got1/Sft2-like vesicle transport protein, which may be located to a late-Golgi
209 compartment and may be involved in the fusion of retrograde transport vesicles derived from an
210 endocytic compartment with the Golgi complex [39]. Likewise, AT4G30240 (hub 19) is a soluble
211 N-ethylmaleimide-sensitive factor attachment protein receptor (SNARE)-like protein harboring a
212 syntaxin-6 domain typical of proteins found in the endosomal transport vesicles [40].

213 Under the biological process ontology, the response to auxin term represented a
214 significantly enriched GO term, which has not been previously associated with begomovirus
215 infection (S2 Table). The NSP-MP-host PPI network uncovered two relevant hubs enriched for
216 auxin response-related proteins, which are represented by an NSP-MP general interaction-derived
217 hub (Fig 1, hub 9) and an NSP-specific host interaction-derived hub (hub 11). Remarkably, these
218 two viral protein hubs are interconnected to each other via interactions with proteins (in gray),
219 which are also over-represented under the auxin response term, forming a large auxin affected hub
220 target by begomovirus (S1 Table). This hub may represent an undocumented biological process
221 affected by begomovirus infection. The resulting PPI network map may provide a framework for
222 future studies in detailing the begomovirus complex life cycle. One such example is described
223 here, as following.

224

225 **A SNARE-like protein designated NSP-Interacting Syntaxin domain-containing Protein**
226 **(NISP), but not its paralog, interacts with NSP via the syntaxin domain**

227 The NSP-MP-Host PPI network uncovered enriched GO terms linked to intracellular
228 vesicle and membrane-bound proteins, which may be associated with a mechanism for
229 intracytoplasmic translocation of viral proteins and vDNA. To pursue further with this possible
230 connection and to validate further the microarray data, we selected a new specific NSP-interacting
231 protein, the SNARE-like protein AT4G30240, which harbors a syntaxin-6 domain at the N-
232 terminus and a transmembrane segment at the C-terminus, for further analyses (Fig 2a). SNARE-
233 complexes drive the fusion of membrane-bound vesicles with target membranes required for
234 intracellular transport via the endosome system. We used the syntaxin domain superfamily as the
235 prototype for the identification of homologs in the genomes of *Arabidopsis thaliana*, *Oryza sativa*,
236 *Drosophila melanogaster*, *Homo sapiens,* and *Saccharomyces cerevisiae*. We then selected the
237 most related proteins to construct phylogenetic trees using Bayesian inference method (S3a Fig).
238 AT4G30240 was clustered in pair with AT2G18860 and formed a clade of syntaxin-6 domain-
239 containing proteins, which also included a third Arabidopsis paralog AT1G27700. This
240 AT4G30240-derived clade (in red), also designated Syntaxin-6-like subgroup, clustered only plant
241 proteins, carrying an N-terminal syntaxin-6-like domain and a C-terminal transmembrane
242 segment. AT4G30240 and AT218860 may be a result of genome duplication, as these syntaxin-6-
243 like proteins clustered in pair even in phylogenetic analyses that include proteins from other
244 organisms, share a high degree of sequence conservation and display similar intron/genomic DNA
245 configuration (https://www.arabidopsis.org/).

246 The remaining syntaxin-6-like proteins clustered together in a distinct clade that included
247 proteins from human, rice and the Arabidopsis AT1G28490, also named SYP61, a characterized
248 trans-Golgi network (TGN)/endosome localized syntaxin [41-43]. This SYP61 second clade (in
249 yellow) was designated target (t)-syntaxin-6/SNARE-like subgroup, as it included structurally
250 similar proteins carrying the N-terminal syntaxin-6 domain and also a tSNARE coiled-coil
251 homology domain at the C-terminus.

252 Due to the lack of a coiled-coil tSNARE domain at C-terminus, the syntaxin-6-like
253 subgroup may represent a new, functionally uncharacterized, plant-specific class of the syntaxin-
254 like family of the t-SNARE superfamily. This hypothesis was further confirmed in a phylogenetic
255 analysis of syntaxin-6 domain-containing proteins from *Arabidopsis thaliana, Oriza sativa*,
256 *Glycine max*, *Zea mays*, *Zostera marina*, *Homo sapiens*, *Mus musculus*, *Bos Taurus*, *Equus*
257 *caballus*, *Danio rerio*, and *Drosophila melanogaster* using the full-length sequence of
258 AT4G30240 as prototype (S3b Fig). This phylogenetic analysis further confirmed that the
259 syntaxin-6 domain-containing proteins form two distinct clades with high internal stability
260 (100%). The AT4G30240-derived clade, syntaxin-6-like clade, includes only plant syntaxin-6-like
261 proteins, and the tSNARE/syntaxin clade includes proteins from all species tested, except yeast.

262 To complement the protein microarray data, we used the yeast two-hybrid to examine
263 further the NSP-AT4G30240 interaction. We also included the paralog AT2G18860 in our assays,
264 which was not present in the protein microarray. The second most closely related paralog,
265 AT1G28490, was present in the protein microarray but was not found to interact with NSP. Co-
266 expression of the full-length AT4G30240 (NISP, NSP-Interacting Syntaxin domain-containing
267 Protein) ORF fused to the activation domain (AD), and NSP fused to the binding domain (BD) of
268 GAL4 promoted histidine prototrophy (Fig 2b). The HIS3 marker gene was not activated in yeast

269 cells cotransformed with the controls. In contrast, AT2G18860 failed to interact with NSP in yeast,
270 as neither AD-AT2G18860 nor BD-AT2G18860 promoted his prototrophy when cotransformed
271 with the respective cognate BD-NSP or AD-NSP (Fig 3c).

272 To map the NSP-interacting domain on NISP, we generated NISP deletion fragments and
273 assay for protein interactions by two-hybrid assay. The N-terminal NISP fragment extending up
274 to amino acid position 107 and containing an intact syntaxin-6 domain ($NISP^{1-107}$, Fig 2a) was
275 sufficient to bind NSP in yeast (Fig 2d). The interaction of the truncated $NISP^{1-107}$ with NSP was
276 specific because the HIS marker gene was not activated in yeast cells co-transformed with AD- or
277 BD-truncated $NISP^{1-107}$ and the empty vectors (Fig 2d). In contrast, the NISP truncated versions,
278 comprising the NISP internal region, delimited by positions 105-200 ($NISP^{105-200}$; Fig 2e) or the
279 C-terminal portion ($NISP^{200-300}$; Fig 2f), were not capable of recognizing NSP, confirming that
280 NISP binds NSP via its syntaxin-6 domain. Although the syntaxin-6 domains of NISP and
281 AT2G18860 are conserved (78.57% identity), NSP interacts specifically with NISP in yeast (Fig
282 2b). Sequence alignment revealed an 8-amino acid deletion at the syntaxin-6 domain of
283 AT2G18860 as the most striking feature that may account for the differences in protein binding
284 specificity (S4 Fig).

285 Although NISP lacks a typical coiled-coil tSNARE domain, it harbors a syntaxin-6 domain
286 at the N-terminus and a predicted transmembrane segment at the C-terminus, which suggests an
287 endomembrane-bound localization (Fig 2a). Mammalian syntaxin-6 domain proteins are localized
288 in the trans-Golgi network (TGN) membranes and endosomal vesicles [44]. To examine the
289 subcellular localization of NISP, we transiently expressed AT4G30240 fused to a green fluorescent
290 protein (GFP) under the control of the native and constitutive promoters, in *Nicotiana benthamiana*
291 leaves and analyzed the localization of the fluorescent signal by confocal microscopy. NISP-GFP

292 was predominantly localized in motile spherical structure, resembling vesicles (Fig 3a, 3b; S1
293 Video). We also examined the localization of the paralog AT2G18860 fused to GFP, which
294 concentrated predominantly in membrane-bound vesicles and plasma membrane (S5 Fig).

295 To examine more precisely the NISP localization, we performed co-localization assays,
296 using SYTA-mCherry as an endosome-associated marker [35], the plasma membrane-associated
297 molecular marker FLS2-mCherry [45], ER-, TGN- and tonoplast-associated molecular markers
298 constructed by Nelson et al. [46]. These co-localization studies showed that NISP-GFP did not co-
299 localize with ER-mCherry- (Fig 3c, asterisks indicate the field of the insets) and tonoplast (vac-
300 mCherry)- (Fig 3e) associated molecular markers. Likewise, NISP-containing vesicles did not co-
301 localize with the plasma membrane FLS2-mCherry (Fig 3f). In contrast, we observed a small
302 population of NISP-GFP-containing vesicles that co-localized with the TGN-associated molecular
303 marker (Fig 3d) and a large fraction of NISP-GFP-containing vesicles precisely co-localizing with
304 the endosomal protein SYTA-mCherry (Fig 3g). Because many of the NISP-labeled vesicles were
305 associated with the plasma membrane, we examined whether the NISP-associated vesicle
306 membrane was derived from the plasma membrane by staining NISP-GFP-expressing cells with
307 FM4-64, a marker for plasma membrane internalization that labels endosomes [47]. In addition
308 to labeling plasma membrane, dye-labeled vesicles were observed that also showed discrete
309 fluorescence with NISP-GFP (Fig 3H). Collectively, these results indicate that NISP localizes in
310 TGN/early endosome vesicles as it co-localized with Golgi-associated markers and endosomal
311 SYTA. Furthermore, the membranes of the NISP-associated vesicles were labeled by FM4-64, a
312 marker for vesicle components of the plant endocytic pathway.

313

314 **NISP interacts with NSP in intracellular vesicles**

315 We next examined whether NISP interacts with NSP *in vivo* using the bimolecular
316 fluorescence complementation (BiFC) assay. The formation of NISP/NSP complexes occurred in
317 vesicles of tobacco epidermal cells independent of the orientation of the NISP fusions (N-terminus
318 or C-terminus of YFP; Fig 4a), and the reconstituted fluorescent signal was much higher than that
319 of the background (control panels with combinations of the protein fusions with empty vectors).
320 The reconstituted fluorescent signal was co-labeled by FM4-64, indicating that the complex was
321 formed in endosomal vesicles derived from the plasma membrane (Fig 4b, see arrows). We further
322 demonstrated that NISP and NSP interacted *in vivo* using co-immunoprecipitation assays. Both
323 NISP-GFP and NSP-6HA, were co-immunoprecipitated from co-infiltrated extracts using anti-
324 GFP antibody, demonstrating a specific association of NISP-GFP with NSP-6HA fusions (Fig 4c).
325 Switching the protein tags did not alter the results because NISP-6HA also associated with NSP-
326 GFP in co-infiltrated extracts (Fig 4d). The Co-IP results also demonstrated that GFP alone did
327 not interact with either NSP-6HA or NISP-6HA, demonstrating the specificity of the interactions
328 between the viral protein and NISP.
329
330 **NISP, but not its paralog AT2G18860, displays a pro-viral function**
331 The biological relevance of the NSP-NISP interactions in begomovirus infection was
332 examined using several different approaches. We first analyzed the expression of NISP from a
333 released microarray data, which showed that NISP was induced by begomovirus infection. This
334 result was further confirmed by quantitative RT-PCR, which also showed that AT2G18860, the
335 NISP paralog that failed to interact with NSP, was not induced by begomovirus infection (S6 Fig).
336 We then identified a T-DNA insertion mutant in the NISP gene (*nisp-1*) and the AT2G18860 gene
337 (*at2g18860-1*). The accumulation of *NISP* and AT2G18860 transcripts in the respective T-DNA

338 insertion mutant was much lower than in Col-0, confirming that *nisp-1* and *at2g18860-1* were loss-
339 of-function mutant lines (Fig 5a, 5b). These mutant lines were complemented by expression of
340 *NISP-GFP* and AT2G18860-GFP in the own knockout background in three independently
341 transformed lines (Fig 5a, 5b, *nisp-1*/NISP lines, and *at2g18860-1/*AT2G18860 lines). We also
342 prepared transgenic lines overexpressing *NISP* and AT2G18860, under the control of a constitutive
343 promoter. The accumulation of NISP and AT2G18860 at transcript (Fig 5a, 5c) and protein (Fig
344 5b, 5d) levels was higher than in Col-0. The knockout and overexpressing lines were
345 phenotypically indistinguishable from Col-0 (S7 Fig).

346 We next examined whether *NISP* and AT2G18860 participate in begomovirus infection.
347 The knockout lines (*nisp-1* and *at2g18860-1),* complemented lines (*nisp-1/NISP* and *at2g18860-*
348 *1/AT2G18860), NISP*-overexpressing lines and Col-O were inoculated with infectious clones of
349 CaLCuV and the course of infection was monitored by visualization of symptom development and
350 PCR diagnosis. The accumulation of viral DNA was quantified by qPCR (Fig 5).

351 The *nisp-1* knockout line displayed attenuated symptoms (Fig 5e), delayed course of
352 infection (Fig 5f), and lower viral DNA as compared to Col-0 (Fig 5g). Expression of NISP-GFP
353 in *nisp-1* restored the wild type susceptibility to begomovirus infection in all three independently
354 transformed lines (*nisp-1/NISP*), confirming that the attenuated susceptibility displayed by the
355 *nisp-1* line was indeed due to loss of *NISP* function. In contrast, *NISP* overexpression conferred
356 enhanced susceptibility to begomovirus infection; the progress of infection was accelerated (Fig
357 5f), and viral DNA load was significantly higher in the *NISP*-overexpressing lines than in Col-0
358 and *nisp-1* lines (Fig 5g). We predicted that if NISP-NSP binding were the bases for the NISP
359 pro-viral function, the closest paralog of NISP, AT2G18860, which harbors the syntaxin-6-like
360 domain but does not interact with NSP, would not affect begomovirus infection. Accordingly, the

361 *at2g18860-1* knockout line, *at2g18860-1/AT2G18860* complemented lines, and an *AT2G18860-*
362 overexpressing line displayed similar symptoms, course of infection and viral DNA load as Col-
363 0, indicating that AT2G18860 does not interfere with begomovirus infection (Fig 5e, 5f, 5g). These
364 results further substantiated the notion that the formation of NSP-NISP complex may be the
365 determinant for the NISP pro-viral function rather than the presence of a syntaxin-6 like domain
366 per se.
367
368 **NISP also interacts with NIG and complex formation is enhanced by viral NSP**
369 There is a gap in our knowledge of how the vDNA-NSP complex, which binds to NIG in
370 the cytosolic side of the nuclear pores, traffics to the cell periphery. From the PPI network map,
371 we hypothesized that NIG could serve as a bridge to attach vDNA to the intracellular transport
372 system of plant cells. The integration of our data with the Arabidopsis interactome uncovered a
373 possible interaction between NIG and NISP, which was also shown here to bind specifically to
374 viral NSP. The interaction between NIG and NISP was first demonstrated by two-hybrid assay
375 (S8 Fig 8a). The co-expression of the NISP ORF fused to BD and NIG ORF fused to AD from
376 GAL4 promoted histidine prototrophy in medium supplemented with 2.5 mM 3AT, whereas co-
377 expression with empty vectors did not.
378 To examine whether NIG and NISP interact *in vivo*, we used BiFC and co-
379 immunoprecipitation assays. NIG has been shown to be unevenly distributed in the cytosol,
380 concentrating around the nuclear envelope (S8b and S8c Fig) [25, 48]. The BiFC data
381 demonstrated that nYFP-NIG is relocated to the vesicle-like compartments via interaction with
382 cYFP-NISP (and vice-versa), as the reconstituted fluorescent signal, which concentrated in
383 membrane-derived vesicles and was barely detected in the controls (Fig 6a), was co-stained by

384 FM4-64 (Fig 6b). The inclusion of NSP-6HA in the BiFC assay increased the NISP-NIG complex
385 formation, as judged by the enhanced intensity of the reconstituted fluorescent signal, showing the
386 fluorescent vesicles associated with the plasma membrane (S9 Fig). To provide further evidence
387 of the NSP-mediated enhancement of NIG-NISP interaction, we used a quantitative co-
388 immunoprecipitation assay (Fig 6, S8 Fig). We first confirmed that NIG interacts with NISP *in*
389 *vivo* (Fig 6c, S8d). The Co-IP results indicated that NISP-GFP, but not GFP alone, interacted with
390 NIG-HA. Likewise, NIG-GFP, but not GFP alone, interacted with NISP-HA. NSP promoted a
391 stronger association of NISP-GFP with NIG-6HA, as judged by the amount of co-
392 immunoprecipitated NIG by anti-GFP in the presence of co-expressed GST-NSP (Fig 6d, 6e).
393 Likewise, GST-NSP enhanced NISP-6HA-NIG-GFP complex formation (S8e and S8f Fig). These
394 results indicate that NSP/NIG and NISP might form a multiprotein complex assembled in
395 intracytoplasmic transporting vesicles. Syntaxin-6 domain-containing proteins have been shown
396 to participate in the endosome-plasma membrane route of protein cargos.
397
398 **NISP complexes viral DNA in vivo**
399 The current model of vDNA intracellular translocation informs that NSP binds to nascent
400 viral DNA in the nucleus, facilitates its translocation to the cytosol via nuclear pores and moves
401 vDNA intracytoplasmically to the cell periphery, where MP mediates the intercellular movement
402 of vDNA-NSP or vDNA-MP via plasmodesmata. Because NSP also binds to NISP in vesicle-like
403 structures, we asked whether the vDNA would be recruited into a NISP multi-protein complex
404 using chromatin immunoprecipitation (ChIP) assay (Fig 7). The untransformed line (Col-0) and
405 NISP-GFP-overexpressing (AtNISP-1, AtNISP-3, and AtNISP-3, Fig 7a) lines were infected with
406 CaLCuV infectious clone and the ChIP assay was performed using an anti-GFP antibody. We

407 confirmed first that the inoculated plants were infected (IN) by performing PCR from input DNA
408 using CaLCuV-specific primers, which amplify a 770-bp fragment from CaLCuV DNA-B (Fig 7b
409 and S10b Fig, primers F1/R1) and a 389-bp fragment from DNA-A (Fig 7e and S10a Fig, primers
410 F1/R1). This viral DNA-B and DNA-A fragments were also amplified from ChIP-DNA of infected
411 (IN) AtNISP-overexpressing lines but not of infected (IN) or uninfected (UN) Col-0, which lacks
412 GFP-tagged NISP (Fig 7a, 7e). Using two sets of DNA-B-specific primers (F2/R2 and F3/R3,
413 S10b Fig), ChIP-qPCR further demonstrated significant enrichment of DNA-B-specific fragments
414 in infected AtNISP-GFP-overexpressing samples, which had been precipitated with anti-GFP
415 serum, but not in pulled down samples from infected Col-0 lines (Fig 7c and 7d). Likewise, the
416 use of F2/R2 set of DNA-A primers (S10a Fig 10a) also resulted in significant enrichment of the
417 DNA-A-specific fragment in ChIPed DNA from infected AtNISP-GFP-overexpressing samples
418 but not from infected Col-0 (Fig 7f). Collectively, our results indicate that NISP is a functional
419 component of the vDNA-complex that traffics along the cytoplasm to the cell periphery for the
420 MP-mediated cell-to-cell movement of vDNA into adjacent cells.
421

422 **Discussion**

423

424 Viruses are obligate intracellular parasites and, once in the host cell cytoplasm, they must
425 move intracellularly to and from the replication site to the plasma membrane for spreading. The
426 cytoplasmic limitations on free diffusion have forced viruses to evolve efficient mechanisms to
427 manipulate the host transport system for their benefit. Understanding how viruses hijack the host
428 intracellular transport system using a limited repertoire of proteins provides an opportunity to
429 uncover the molecular bases of the host transport machinery. Bipartite begomoviruses, plant

430 ssDNA viruses, use two movement proteins, MP and NSP, to move intracellularly from the site of
431 replication in the nucleus to the cell surface [17]. However, the host components of the vDNA
432 complex competent for intracytoplasmic translocation have not been identified, and the underlying
433 mechanism for intracytoplasmic trafficking of vDNA remains to be elucidated. Here, we used a
434 previously fabricated, *in situ* synthesized protein microarray containing 4600 Arabidopsis ORFs
435 [37] to identify NSP- and MP-Arabidopsis protein-protein interactions (PPIs). Consistent with the
436 movement function of the viral proteins, the identified NSP-MP-PPI network uncovered direct and
437 indirect interactions, over-represented under transport activity, protein binding, membrane-bound
438 organelles, intracellular vesicle, and SNARE complex ontology terms, which may define an
439 intracellular route for vDNA trafficking. Precedents in the literature have implicated a
440 microtubule-associated intracellular movement of viral proteins and vDNA in addition to an
441 endocytic recycling pathway for the MP-mediated cell-to-cell movement of vDNA protein
442 complexes (35; 36]. Accordingly, transport function-related proteins, including kinesin motor
443 protein, plant syntaxin 121, Rab GTPase, Ras, Got1/Sft2-like vesicle transport protein, target
444 SNARE coiled-coil domain protein, syntaxin-6 plant proteins, prenylated Rab acceptor, Heat
445 shock protein 70 (Hsp 70), nuclear pore anchor, synaptotagmin A, were over-represented in the
446 MP-NSP- PPI network. These studies thus provided a critical framework for future investigations
447 to elucidate the molecular mechanisms for intracytoplasmic transport of begomoviruses.
448

449 **The NSP-interacting syntaxin domain-containing protein (NISP) is identified as a new**
450 **functional cellular partner of begomovirus NSP**

451 In the present investigation, we characterized an NSP-specifically interacting syntaxin-6
452 domain-containing protein, designated NISP and provided several lines of evidence indicating that

453 NISP might be involved in the intracytoplasmic movement of NSP-vDNA. First, co-localization
454 studies using organelle-associated molecular markers, and the FM4-64 marker demonstrated that
455 NISP is associated with TGN/early endosomal vesicles. Second, we confirmed that NISP
456 interacted with NSP *in planta* and showed that the complex formation occurred in vesicle-like
457 structures, which resemble the NISP-associated TGN/endosomal vesicles, the typical subcellular
458 localization of syntaxin-6-like proteins from Arabidopsis and humans [49]. Third, we showed that
459 NISP exhibits a pro-viral function, and begomovirus infection required NISP-NSP interaction. The
460 mutant *nisp-1* was resistant to begomovirus as the knockout lines displayed attenuated symptoms,
461 a delayed course of infection, and accumulated much lower viral DNA as compared to Col-0. In
462 contrast, the overexpressing lines were hypersensitive to begomovirus. We took advantage of a
463 highly conserved NISP paralog, AT2G18860, to show that NISP-NSP interaction was the
464 molecular basis for the NISP pro-viral function. AT2G18860, which shares with NISP a 78,6%
465 identical syntaxin-6 domain, did not interact with NSP and thus did not interfere with begomovirus
466 infection. Consistent with these data, NISP, but not AT2G18860, is induced by begomovirus
467 infection. Fourth, NISP also interacted with NIG, which facilitates the release of the NSP-DNA
468 complex from the nuclear pores to the cytosol [12,18], and the presence of NSP enhanced the
469 NISP-NIG complex formation, indicating that NSP, which interacts with NIG [12] and NISP (Fig
470 4), may be recruited by the complex. We used ChIP assay to demonstrate that NISP was also
471 associated with vDNA in infected cells, which may be assembled into a NISP-NIG-NSP
472 multiprotein complex. Finally, the NISP interactions relocated the dispersed cytosolic NIG and
473 viral NSP to trafficking vesicle resembling the NISP-containing spherical structure associated with
474 TGN/endosome. The NISP-mediated translocation of NSP-vDNA to endosomal vesicles favors
475 the association of the viral complex with MP, which is brought to the endosome via interaction

476 with the endosome-associated SYTA for the MP-mediated cell-to-cell movement of vDNA [35].

477

478 **NISP belongs to a new, previously unidentified plant-specific subfamily of syntaxin-6-like**
479 **proteins**

480 The phylogenetic reconstruction of syntaxin-6 domain-containing proteins from different
481 eukaryotic organisms divided this family into two subclades, one containing proteins from all
482 tested organisms, including SYP61 from Arabidopsis, and a new, previously unidentified plant-
483 specific subclade, which includes NISP and AT2G18860 paralogs clustered in pair. SYP61 has
484 been shown to form functional SNARE complexes involved in the vacuolar-TGN recycling
485 pathway and in exocytotic trafficking to the plasma membrane [43,50]. The process of membrane
486 fusion is the final step of vesicle transport, which is generally driven by a specific pairing of 1 v-
487 SNAREs with the 3 or 3 cognate t-SNARE molecules into a trans-SNARE complex [49, 51]. The
488 proteins from the SYP61 subclade contain the typical structural configuration of t-SNARES,
489 including the N-terminal syntaxin-6 domain, followed by a C-terminal t-SNARE coiled-coil
490 homology domain and a transmembrane segment at the C-terminus. The proteins from the NISP
491 subclade harbor the N-terminal syntaxin-6 domain and the transmembrane segment but lack a C-
492 terminal SNARE domain, which may impair the participation of these new syntaxin-6-like proteins
493 in the assembly of a functional trans-SNARE complex for membrane fusion. Nevertheless, we
494 have demonstrated that a representative of this new syntaxin-6 subclade, NISP, is functionally
495 expressed in plant cells. In addition to being induced by begomovirus infection, NISP functions as
496 a susceptibility factor to begomoviruses, forms complexes with viral and host proteins and is
497 located in TGN/endosome-associated vesicles. We also mapped the NSP-binding domain on NISP
498 to the syntaxin-6 domain. Therefore, we propose that NISP may function as an intracellular vesicle

499 docking site to which the cargo proteins are specifically recruited through interactions with the
500 syntaxin-6-like domain.

501 We also showed that members of the new syntaxin-6 subclade might diverge functionally
502 concerning protein-protein binding specificity. The NISP paralog, AT218860, which shares with
503 NISP a conserved syntaxin-6 domain (78.6% identity), fails to interact with viral NSP and hence
504 does not affect begomovirus infection. Therefore, specificity of protein interactions may rely on
505 marginal features of the syntaxin-6 domain. A striking difference between NISP and AT2G18860
506 is an eight-amino acid deletion toward the N-terminus of the syntaxin-6 domain, which may
507 account for the NISP specificity to NSP (S4 Fig). Complementary studies are necessary to
508 precisely define the determinants of a functional syntaxin-6 domain for NSP interaction, which
509 will be useful for engineering resistance to begomoviruses.

510

511 **NISP may participate in the intracytoplasmic transport of NSP-vDNA**

512 Based on the current data and others previously reported data, we propose a model for the
513 NISP integration into an intracytoplasmic transport route used for the begomovirus anterograde
514 movement. Begomoviruses replicate in the nuclei of infected cells, where NSP interacts with
515 newly-synthesized vDNA and facilitates the translocation of vDNA to the cytoplasm via nuclear
516 pores [13, 32]). This nuclear exportation process may be mediated by an exportin-like protein yet
517 to be identified. At the cytosolic side of the nuclear envelope, NIG associates with the NSP-vDNA
518 complex to accessorize the release of NSP-vDNA from the nuclear pores into the cytosol [12,18].
519 The pro-viral function of NIG is associated with its cytosolic localization because the WWP1-
520 mediated recruitment of NIG into nuclear bodies impairs begomovirus infection [48]. At the
521 cytosol, we showed here that NISP may recruit the NIG-NSP-vDNA complex to TGN/endosome-

522 associated transport vesicles. The nature of the NISP-associated vesicle was identified using cell
523 biology molecular markers and FM4-64, which demonstrated that NISP is predominantly localized
524 at TGN and in the early endosome (Fig 3), which was consistent with the localization of syntaxin-6
525 proteins in most eukaryotic cells [40]. As MP has been demonstrated to associate with the
526 endosomal SYTA, a possible NISP sequestration of NSP-DNA into TGN/endosome-associated
527 vesicles may provide the means for the predicted interactions between endosomally localized MP-
528 SYTA and NSP-DNA, which would favor the MP-mediated intercellular transport of vDNA via
529 an endocytic recycling pathway [35]. In summary, our data support a model in which direct
530 interactions between the host factor NISP and NIG/NSP modulate vDNA intracellular trafficking
531 to endosomes where MP, recruited by the endosomal SYTA, opportunistically interacts with NSP-
532 vDNA to mediate the cell-to-cell movement of vDNA via plasmodesmata.
533

534 ## Material and Methods

535

536 **Phylogenetic analysis**

537 The amino acid full-length sequences of plant proteins were retrieved from TAIR
538 (http://arabidopsis.org/), Phytozome v12 database (https://phytozome.jgi.doe.gov/) and amino acid
539 full-length sequences of other species from the Ensemble database
540 (https://www.ensembl.org/index.html). The syntaxin domain superfamily was predicted using the
541 software HMMER v3.2.1 (http://hmmer.org/) using Pfam v.30 database (https://pfam.xfam.org/).
542 The syntaxin domain-containing protein sequences were selected to perform the phylogenetic
543 reconstruction. The amino acid sequences were aligned using the MUSCLE algorithm [51].
544 Phylogenetic trees were constructed using Bayesian Inference with MrBayes v3.2.2 [52] and mix

545 model of amino acid substitution (Wag). The analyses were performed running 10.000.000
546 generations and excluding the first 2.500.000 generations as burn-in and visualized with Figtree
547 software (http://tree.bio.ed.ac.uk/software/figtree/). Plant NISP homologous proteins were
548 identified using the BLAST algorithm implemented in the Ensemble and Phytozome databases.
549 The amino acid sequences of the NISP homologs were selected for phylogenetic reconstruction of
550 N-terminal Syntaxin-6 family using the same tools and criteria applied for the superfamily syntaxin.
551 However, the amino acid substitution model Jones was used for the N-terminal Syntaxin-6
552 phylogenetic tree.
553
554 **PPI network analysis**
555 NSP- and MP-interacting proteins from Arabidopsis were used as a query term to identify
556 their respective interactions described in the BAR database (Bio-Analytic Resource for Plant
557 Biology, http://bar.utoronto.ca/interactions/). The Biogrid and IntAct databases were selected for
558 searching. The protein-protein interactions (PPI) were retrieved and imported into the Cytoscape
559 software (https://cytoscape.org/) to visualize the topology of the PPI network and to calculate the
560 network centrality metrics for each protein. The measured network centralities were betweenness,
561 closeness, eccentricity, and degree. Briefly, the betweenness centrality in the PPI network of the
562 graph G = (V,E) was calculated by observing the number of times a node v (protein) contributes
563 as a link along the shorter paths among all nodes. The betweenness centrality of this node can be
564 analyzed as:

565
$$\sum_{s,t \in V} \frac{\sigma(s,t|v)}{\sigma(s,t)}$$

566 where V is the total set of nodes, $\sigma(s,t)$ is the number of shorter paths of (s,t), and $\sigma(s,t|v)$ is the
567 number of paths crossing v [53]. The betweenness centrality can indicate the relevance of a protein

568 as functionally capable of keeping together interacting proteins. Closeness centrality (of a node v
569 is the sum of the shortest path distances from w to all other nodes and calculated as described by
570 Freeman [54]:
571
572 $$\frac{1}{\sum_{w \in V} dist(v, w)}$$
573
574 A high closeness value can be determined by the fact that all nodes are usually close to node v.
575 The eccentricity centrality of a node v is the maximum distance from v to all other nodes in graph
576 G and can be analyzed as described by Hage and Harary [55]:
577
578 $$\frac{1}{max\{dist(v, w) : w \in V\}}$$
579

580 In addition, the degree centrality of node *v* was calculated by $\sum i{=}1^{K} di$, where *d* represents each
581 adjacent node and *K*, the total number of adjacent nodes. Nodes with a high degree can be
582 designated hubs and hold together different nodes with a lower degree.

583 **GO analysis of the PPI network**

584 The gene set enrichment analysis (GSEA) of the proteins that compose the PPI network
585 was performed using the Bioconductor GOstats package [56]. GSEA analysis computes
586 hypergeometric test p values for over- or underrepresentation for each GO term, and the annotation
587 of genes is based on the Bioconductor annotation package org.At.tair.
588

589 **Plasmid constructions**

590 All recombinant plasmids were generated by the GATEWAY cloning system (Invitrogen,
591 http://www.invitrogen.com/). The primers used for gene amplification are listed in S3 Table. The
592 coding regions of *NISP* (AT4G30240) and AT2G18860, with or without a translational stop codon,
593 were amplified from leaf cDNA of *Arabidopsis thaliana* ecotype Columbia (Col-0) and inserted
594 into the entry vectors pDONR201 and pDONR207. The resulting clones were designated
595 At4g30240-St-pDONR201 (pUFV2134), At4g30240-Ns-pDONR201 (pUFV2135), At2g18860-
596 St-pDONR201 (pUFV3193), At2g18860-Ns-pDONR201 (pUFV3194), At4g30240-St-
597 pDONR207 (pUFV2236), At4g30240-Ns-pDONR207 (pUFV2237), At2g18860-St- pDONR207
598 (pUFV3195), At2g18860-Ns-pDONR207 (pUFV3196). Then, the DNA inserts were transferred
599 by recombination from the entry vector to different yeast and plant expression vectors.

600 For the yeast two-hybrid assay, the *NISP* and AT2G18860 coding regions were transferred
601 from the respective entry vectors (At4g30240-St-pDONR201 and At2g18860-St-pDONR201) to
602 the yeast expression vectors pDEST32 and pDEST22, generated the clones At4g30240-St-
603 pDEST32 (pUFV2141), At4g30240-St-pDEST22 (pUFV2142), At2g18860-St-pDEST32
604 (pUFV3197) and At2g18860-St-pDEST22 (pUFV3198), fused to binding domain (BD)
605 (pDEST32) or activation domain (AD) (pDEST22) of GAL4. The *NSP*- and *NIG*-derived clones
606 used in the yeast two-hybrid assay have been previously described and designated NSP-St-
607 pDEST32, NSP-Cl-pDEST22 (Fontes *et al*., 2004), and NIG-pDEST22 (pUFV2547; Calil *et al*.,
608 2018).

609 For the subcellular localization experiments, the *NISP* and AT2G18860 coding region were
610 fused to GFP and expressed in planta under the control of the CaMV 35S promoter in the vector
611 pK7FWG2. For the co-immunoprecipitation assay, in addition to the GFP fusion, *NISP* ORF was
612 also fused to hemagglutinin (HA) tag, using the binary destination vector pK7m34GWfor three

613 fragment recombination. The resulting DNA constructions were At4g30240-pK7FWG2
614 (pUFV2576), At2g18860-pK7FWG2 (pUFV3199) and 2x35S::At4g30240-Ns-6HA-pH7m34GW
615 (pUFV2586).

616 For the subcellular co-localization assays, the ER-associated molecular marker ER-
617 mCherry (CD-959), the TGN-associated molecular marker G-mCherry (CD-967) and the
618 tonoplast-associated molecular marker vac-mCherry (CD-975) were obtained from the
619 Arabidopsis Biological Resource Center. The plasma membrane-associated molecular marker,
620 FLS2-mCherry was obtained by amplifying the *FLS2* ORF from Arabidopsis cDNA with the
621 primers AtFLS2-Fwd and AtFLS2-NS-Rvs (S3 Table), inserting the amplified fragment by
622 recombination into pDON207 and transferring it by triple recombination to the destination vector
623 pH7m34GW along with FLS2-Ns-pDON207, pDONR-P4-P1R+2x35S, and pDONR-P2R-
624 P3+mCherry, resulting in the clone FLS2-mCherry (pUFV3034). Likewise, the SYTA ORF was
625 amplified from leaf cDNA with the primers AtSYTA-Fwd and AtSYTA-NS-Rvs (S3 Table),
626 cloned into the entry vector pDONR-207 and transferred via triple recombination to the destination
627 vector pH7m34GW along with SYTA-NspDON207, pDONR-P4-P1R+2x35S, and pDONR-P2R-
628 P3+mCherry, generating SYTA-mCherry (pUFV3296).

629 The *NISP* coding region was also fused to GFP and expressed in plants under the control
630 of its endogenous promoter. For this, about 2000 bp of 5' flanking sequence of At4g30240 was
631 PCR-amplified using the primers described in S3 Table and cloned into pDONR-P4-P1R, yielding
632 proAt4g30240-pDONR-P4-P1R (pUFV2436). Then, the 5' flanking sequence was transferred by
633 triple recombination to the destination vector pK7Fm34GW along with At4g30240-Ns-pDON201,
634 proAt4g30240-pDONR-P4-P1R, and eGFP-pDONR-P2R-P3, resulting in the clone
635 At4g30240::At4g30240-GFP (pUFV2849). The *NSP*- and *NIG*-derived clones used for co-

636 immunoprecipitation assays have been previously described and designated as 2x35S-NSP-Cl-
637 6HA-pH7m34GW (pUFV2424), NSP-Cl-pK7FWG2(pUFV2536), 2x35S-NIG-Ns-6HA-
638 pH7m34GW (pUFV1946) and NIG- pK7FWG2 (pUFV1177) [48].

639 The SPYNE-GW and SPYCE-GW vectors, which contain the N-terminal (nYFP) and C-
640 terminal (cYFP) of YFP, respectively, were used for the BiFC experiments. At4g30240-Ns-
641 pDONR207 was transferred to SPYNE-GW and SPYCE-GW, yielding At4g30240-Ns-SPYNE
642 (pUFV2238) and At4g30240-Ns-SPYCE (pUFV2239). The *NSP*- and *NIG*-derived clones used in
643 the BiFC assays have been previously described and designated as NSP-Cl-Ns-SPYNE
644 (pUFV1654), NSP-Cl-Ns-SPYCE (pUFV1655), NIG-Ns-SPYNE (pUFV1646), and NIG-Ns-
645 SPYCE (pUFV1647) [48].

646 NISP truncated versions were obtained from At4g30240-St-pDONR201 by PCR using
647 primers listed in S3 Table. The generated fragments were cloned into the entry vector pDONR201
648 and designated as At4g30240(1-107)-St-pDONR201 (pUFV2806), At4g30240(105-200)-St-
649 pDONR201 (pUFV2807) and At4g30240(200-300)-St-pDONR201 (pUFV2808). The respective
650 DNA inserts were then transferred to the yeast expression vectors, yielding At4g30240(1-107)-St-
651 pDEST32 (pUFV2822), At4g30240(1-107)-St-pDEST22 (pUFV2819), At4g30240(105-200)-St-
652 pDEST32 (pUFV2823), At4g30240(105-200)-St-pDEST22 (pUFV2820), At4g30240(200-200)-
653 St-pDEST32 (pUFV2824) and At4g30240(200-300)-St-pDEST22 (pUFV2821).

654

655 **Detecting MP- and NSP-host protein interactions on high-density halo tag-NAPPAs**

656 The identification of NSP and MP partners was carried out through a previously fabricated
657 high-density HaloTag nucleic acid programmable protein array (HaloTag-NAPPA), as described
658 by Yazaki *et al*. [37]. The protein microarray, which consisted of a set of *in situ* synthesized

659 proteins from 4600 *Arabidopsis thaliana* ORFs, has been designated AtNAPPA01. 3×HA-fused
660 CaLCuV MP and NSP proteins were independently expressed using the TNT system (Promega)
661 according to the manufacturer's recommendations. The *in vitro* synthesized HA-fused MP, and
662 HA-fused NSP were used to probe individually AtNAPPA01. The identification of MP- and NSP-
663 interacting proteins with the NAPPA protein-protein interaction method was from a single
664 experiment using duplicated spots on one glass slide. Interactions were considered positive only
665 when both replicated spots displayed normalized signal intensity above background. Experiments,
666 data scanning, quantification, and data processing were carried out as described by Yazaki *et al*.,
667 2016.
668
669 **Plant growth conditions and transformation**
670 *Arabidopsis thaliana*, ecotype Columbia (Col-0), was used as the wild type. Homozygous
671 seeds from the T-DNA insertional mutants *nisp-1* (Salk_117751) and *at2g18860-1* (Salk_099699)
672 were obtained from the Arabidopsis Biological Resource Center. Arabidopsis seeds were surface-
673 sterilized and cold treated at 4°C for 72 h in the dark and then exposed to white light. Seedlings
674 were grown at 22°C on plates containing Murashige-Skoog (MS) medium for 2 weeks and then
675 transferred to soil. Plants were grown in a growth chamber at 22 ºC under short-day conditions
676 (12h light/12h dark). Transgenic lines were obtained via *A. tumefaciens*-mediated transformation
677 using the floral dip method [57]. Transformed plants with the indicated DNA constructions were
678 selected in MS medium supplemented with the appropriate antibiotic (kanamycin, pK7FWG2).
679 Selected transformants were confirmed by PCR, transferred to soil, and grown in a growth
680 chamber at 22 ºC under long-day conditions (16h light/8h dark) to generate seeds. For segregation
681 analysis, seeds were germinated on MS medium containing 50 μgmL^{-1} kanamycin. Homozygous

682 T1 lines for the T-DNA loci were selected by determining the frequency of their kanamycin-
683 resistant T2 seeds after self-pollination. Accumulation of NISP-GFP and AT2g18860-GFP
684 transcript and protein levels were monitored in each generation by qRT-PCR using gene-specific
685 primers (S3 Table) and immunoblotting using anti-GFP antibody. From the independently
686 transformed lines (8-15 lines of each construct and genotype transformed), we selected three
687 independently transformed lines which appeared to have an integrated T-DNA locus on a single
688 chromosome, since 75% of their T1 segregating seedlings were resistant to kanamycin (S4 Table).
689 The selected lines are presented in S4 Table. The nomenclature *nisp*-1/NISP-1-3 indicates that the
690 genotype *nisp-1* was transformed with At4g30240-pK7FWG2, harboring the *NISP* ORF fused to
691 the N-terminus of GFP under the control of the 35S promoter to generate NISP-complementing
692 lines. The designations AtNISP-1, AtNISP-2 and AtNISP-3 indicate three independently
693 transformed lines, which were generated by transformation of Col-0 with At4g30240-pK7FWG2
694 to obtain NISP-GFP-overexpressing lines. The same nomenclature was applied for the
695 transformation of *at2g18860-1* mutant and Col-0 with At2g18860-pK7FWG2, containing the
696 At2g18860 ORF fused to the N-terminus of GFP under the control of 35S promoter (S4 Table).
697

698 **RNA isolation and qRT-PCR analysis**

699 Primers were designed using the Primer Express 3.0 (Life Technologies). Total RNA was
700 extracted from Arabidopsis leaves using TRIzol reagent (Thermo Fisher Scientific) and quantified
701 with a NanoDrop spectrophotometer. Total RNA (2 μg) was treated with RNase-free DNase I and
702 reverse transcribed using oligo (dT) (0,5 μM) and 1U of M-MLV (Thermo). Real-time RT-PCR
703 was carried out using SYBR Green PCR Master Mix (Life Technologies), DNA template, and
704 primers in 10 μL of reaction and an ABI7500 real-time PCR system (Life Technologies). The

705 expression of each gene was normalized to the expression of *Actin* and quantified using the $2^{-\Delta Ct}$
706 method. The primers used to detect specific transcripts with real-time RT-PCR are listed in S3
707 Table.
708
709 **Yeast two-hybrid assay**
710 Competent cells of *Saccharomyces cerevisiae*, strain AH109 (MATa, trp1-901, leu2-3,
711 112, ura3-52, his3-200, gal4Δ, gal80Δ, LYS2::GAL1UAS-GAL1TATA-HIS3, GAL2UAS-
712 GAL2TATA-ADE2, URA3::MEL1UAS-MEL1 TATA-lacZ), were cotransformed with the yeast
713 expression vectors pDEST22 (Gal4 AD) and pDEST32 (Gal4 BD), carrying the coding region of
714 the tested proteins, along with 100 µg of salmon sperm carrier DNA (ssDNA), using the lithium
715 acetate/polyethylene glycol (PEG) method (Gietz and Woods, 2002). For the selection of double
716 transformants, the cells were plated on medium deficient in leucine and tryptophan (SD, Synthetic
717 Dropout, -Leu, -Trp) and cultured for 4 days at 28°C. Interactions were monitored by the ability
718 of the reporter strain to grow on media lacking leucine, tryptophan, and histidine but supplemented
719 with 2.5 mM 3-AT (3-Amino-1,2,4-triazole; Sigma) for 4 days at 28°C.
720
721 **Co-immunoprecipitation assay**
722 The *in vivo* interactions between NISP and NSP or NIG were monitored by co-
723 immunoprecipitation using the µMACS™ Epitope Tag Protein Isolation (MACS/Miltenyil Biotec)
724 kit, according to manufacturer's recommendations. *Agrobacterium tumefaciens (strain GV310)*-
725 mediated transient expression in *N. benthamiana* leaves was carried out as described (Carvalho et
726 al. 2008b). Total protein extracts were obtained from infiltrated leaves expressing the recombinant
727 proteins and incubated for 2 h with anti-green fluorescent protein (GFP) magnetic beads (MACS

728 / Miltenyi Biotec) at 4 ºC under rotation. After incubation, the extracts were applied to a MACS
729 column for the indicated protein tag, washed five times before elution with a pre-heated buffer at
730 95 ºC. The immunoprecipitated proteins were separated by sodium dodecyl sulfate-
731 polyacrylamide gel electrophoresis (SDS-PAGE) 10% (p/v), immunoblotted with the monoclonal
732 antibodies anti-human influenza hemagglutinin (anti-HA) epitope tag, amino acids 98-106
733 (Miltenyi Biotec, 130-091-972) or anti-GFP (Miltenyi Biotec, 130-091-833), and detected using
734 Signal West Pico Chemiluminescent Substrate (Thermo Scientific) according to the
735 recommendations of the manufacturer.
736
737 **Bimolecular fluorescence complementation (BiFC) assay**
738 Different combinations of *A. tumefaciens* strain GV3101 expressing the indicated proteins
739 fused to N-YFP/C-YFP were co-infiltrated into the abaxial surface of *N. benthamiana* leaves at
740 OD_{600nm} of 1:1 proportion. Three days after infiltration, fluorescence was examined in epidermal
741 cells using a Zeiss inverted 510 META laser scanning microscope equipped with an argon laser
742 and a helium laser as excitation sources. YFP was excited at 514 nm using the argon laser, and
743 YFP emission was detected using a 560–615-nm filter. The images were processed using LSM
744 Image Browser 4 (ZEISS) software.
745
746 **Subcellular localization**
747 The subcellular localization of proteins was examined in epidermal cells of *N. benthamiana*
748 leaves transiently expressing GFP fusions. Briefly, *N. benthamiana* leaves were agro-infiltrated
749 with *A. tumefaciens* strain GV3101 carrying proAt4g30240-pDONR-P4-P1R (pUFV2436),
750 At4g30240-pK7FWG2 (pUFV2576) or At2g18860-pK7FWG2 (pUFV3199) (Method S1) and

751 fluorescence of the GFP fusions were visualized in epidermal cells 3 days after infiltration by
752 confocal microscopy using a Zeiss inverted 510 META laser scanning microscope equipped with
753 an argon laser and a helium laser as excitation sources. GFP was excited by the argon/helium-neon
754 laser system in 488 nm wavelength, and emission was collected in 500–530 nm band-pass filter.
755 Images were captured and processed with LSM Image Browser 4 (Carl-Zeiss) software.

756 For co-localization assays, NISP-GFP was co-expressed with ER-, Golgi-, tonoplast-,
757 plasma membrane- and endosome-associated molecular markers fused to mCherry (see in plasmid
758 constructions) and fluorescence was examined by confocal microscopy, using a Zeiss inverted
759 LSM510 META laser scanning microscope, on whose system, the default scanning mode is
760 sequential scanning (multitrack mode). For imaging GFP, the 488 nm excitation line and the 500
761 to 530 nm band pass filter were used. Excitation of mCherry was at 540 nm and emission of 608-
762 680 nm. For the FM4-64 staining, 48 h after agro-infiltration with the DNA construct expressing
763 NISP-GFP, the leaves were infiltrated with a solution of 50 μM FM4-64 (Molecular Probes,
764 Eugene, OR) and examined by confocal microscopy 1h post-infiltration.

765

766 **Infectivity assay**

767 The generation of transgenic lines overexpressing NISP (AtNISp) and At2g18860
768 (AT2G18860), knockout lines (*nisp-1* and *at2g18860-1*), NISP complementing lines are described
769 in Method S1. Transgenic lines and Columbia at the seven-leaf stage were inoculated with
770 plasmids containing partial tandem repeats of CaLCuV DNA-A and DNA-B by biolistic delivery
771 using a microprojectile bombardment model PDS-1000/He accelerator at 900 psi. (24, 26, 58). The
772 inoculated plants were transferred to a growth chamber and monitored for symptoms development
773 and progress of infection [23, 59]. Total DNA was extracted from systemically infected leaves

774 [60], and viral DNA accumulation was detected by PCR using universal DNA-B specific primers
775 PBL1v2040 and PCRC1 [61] (S3 Table). In each experiment, 15 plants of each line were
776 inoculated with 2 μg of tandemly repeated DNA-A plus DNA-B per plant. The course of infection
777 was examined using data from three independent experiments.
778
779 **Quantification of viral DNA in infected plants**
780 The accumulation of viral DNA in infected plants was quantified by qPCR [26]. The
781 reactions were prepared in 10 μL using SYBR Green Master Mix (Life Technologies), 100 ng of
782 total DNA from systemically infected leaves, and CaLCuV-DNA-B-specific primers (S3 Table),
783 and analyzed on a real-time PCR system. The genomic copies of CaLCuV were normalized against
784 an internal control (18S rRNA) to account for template input variation between tubes. For viral
785 DNA quantification, standard curves were prepared using serial dilutions of DNA-B of CaLCuV
786 (100 to 10^6 copies of viral genome per reaction).
787
788 **Chromatin immunoprecipitation (ChIP) assay**
789 The *in vivo* interaction between NISP and viral DNA was evaluated by ChIP. NISP-
790 overexpressing transgenic lines (AtNIS) and Columbia (Col-0) at the six-leaf stage were
791 inoculated by biolistic delivery with CaLCuV DNA-A and DNA-B infectious clones. Tissue
792 harvest, isolation of nuclei, and chromatin breaks from 45 days-old infected plants were conducted
793 according to Alves et al. [62] and Yamaguchi et al. [63]. The chromatin immunoprecipitation was
794 carried out with 1 μl of polyclonal anti-GFP serum (Life Technologies A11122; 3x diluted).
795
796 **ChIP-qPCR**

797 NSP primers (S3 Table) were initially used to amplify viral DNA-B from the
798 immunoprecipitated DNA and input DNA to ensure DNA-B-specific amplification in samples.
799 Likewise, DNA-A-specific primers were used to examine initial amplification of the DNA-A
800 component. Each reaction contained 1 µL of immunoprecipitated DNA or 20-fold diluted input
801 DNA, 0,2 mM CaLCuV-DNA-B-specific primers (S3 Table), and 5 µL of SYBR Green PCR
802 Master Mix (Life Technologies) in 10 µL total volume. The thermal cycling conditions of the
803 reactions consisted of an initial step at 95°C for 10 min, followed by 40 cycles at 94°C for 15 s
804 and 58°C for 45 s. The cycle threshold (Ct) values from Col-0 and AtNISP were normalized with
805 the Ct values of the respective inputs, and the results were expressed as a percentage of the input.
806

807 **Author Contribution**

808 B.C.G.M performed most of the experiments; L.G.C.M. performed the co-localization
809 experiments and protoplast protein localization assays; M.D.-B. performed protein microarray
810 assay; B.C.G.M. and J.P.B.M. performed two hybrid assays; J.C.F.S. performed *in silico* and
811 statistical analyses; B.C.G.M. and A.A.S. performed BiFC assays; E.P.B.F. and J.R.E. conceived
812 experiments; B.C.G.M. and E.P.B.F. designed all experiments, analyzed the data and wrote the
813 manuscript.
814

815 **Acknowledgments**

816 The authors are grateful to the microscopy facility at Universidade Federal de Viçosa.
817

818 **Funding**

We are grateful to the Brazilian funding agencies CAPES, CNPq, FAPEMIG, and the National Institute of Science and Technology in Plant-Pest interactions for supporting this study.

Competing interests

The authors have declared that no competing interests exist.

References

1. Dodding MP, Way M. Coupling viruses to dynein and kinesin-1. EMBO J. 2011;30: 3527-3539.

2. Schoelz JE, Harries PA, Nelson RS. Intracellular transport of plant viruses: finding the door out of the cell. Mol Plant. 2011;4: 813-831.

3. Harries PA, Schoelz JE, Nelson RS. Intracellular Transport of Viruses and Their Components: Utilizing the Cytoskeleton and Membrane Highways. Mol Plant-Microbe Interac. 2010;23: 1381-1393.

4. Wolf S, Deom CM, Beachy RN, Lucas WJ. Movement protein of tobacco mosaic virus modifies plasmodesmatal size exclusion limit. Science. 1989;246: 377-379.

5. Arriagada G. Retroviruses and microtubule-associated motor proteins. Cell Microbiol. 2017;19: e12759.

6. Rojas MR, Macedo MA, Maliano MR, Soto-Aguilar M, Souza JO, Briddon RW, et al. World Management of Geminiviruses. Ann Rev Phytopathol. 2018;56: 637-677.

7. Hanley-Bowdoin L, Bejarano ER, Robertson D, Mansoor S. Geminiviruses: masters at redirecting and reprogramming plant processes. Nat Ver Microbiol. 2013;11: 777-788.

8. Silva JCF, Carvalho TFM, Basso MF, Deguchi M, Pereira WA, Sobrinho RR, et al. Geminivirus data warehouse: a database enriched with machine learning approaches. BMC Bioinformatics. 2017;18: 240.

844 9. Pascal E, Sanderfoot AA, Ward BM, Medville R, Turgeon R, Lazarowitz SG. The geminivirus
845 BR1 movement protein binds single-stranded DNA and localizes to the cell nucleus. Plant Cell.
846 1994;6: 995-1006.
847 10. Rojas MR, Noueiry AO, Lucas WJ, Gilbertson RL. Bean dwarf mosaic geminivirus movement
848 proteins recognize DNA in a form- and size-specific manner. Cell. 1998;95: 105-113.
849 11. Hehnle S, Wege C, Jeske H. Interaction of DNA with the movement proteins of geminiviruses
850 revisited. J Virol. 2004;78: 7698-7706.
851 12. Carvalho CM, Fontenelle MR, Florentino, LH, Santos AA, Zerbini FM, Fontes EPB. A novel
852 nucleocytoplasmic traffic GTPase identified as a functional target of the bipartite geminivirus
853 nuclear shuttle protein. Plant J. 2008a;5: 869-880.
854 13. Sanderfoot AA, Lazarowitz SG. Cooperation in viral movement: The geminivirus BL1
855 movement protein interacts with BR1 and redirects it from the nucleus to the cell periphery. Plant
856 Cell. 1995;7: 1185-1194.
857 14. Noueiry AO, Lucas WJ, Gilbertson RL. Two proteins of a plant DNA virus coordinate nuclear
858 and plasmodesmatal transport. Cell. 1994;76: 925-932.
859 15. Lazarowitz SG, Beachy RN. Viral movement proteins as probes for intracellular and
860 intercellular trafficking in plants. Plant Cell. 1999;11: 535-548.
861 16. Ward BM, Lazarowitz SG. Nuclear export in plants: use of geminivirus movement proteins
862 for a cell-based export assay. Plant Cell. 1999;11: 1267-1276.
863 17. Gafni Y, Epel BL. The role of host and viral proteins in intra and inter-cellular trafficking of
864 geminiviruses. Physiol Mol Plant Pathol. 2002;60: 231-241.
865 18. Carvalho CM, Machado JP, Zerbini FM, Fontes EP. NSP-interacting GTPase: a cytosolic
866 protein as cofactor for nuclear shuttle proteins. Plant Signal Behav. 2008b;3: 752-754.

867 19. Sanchez-Velar N, Udofia EB, Yu Z, Zapp ML. hRIP, a cellular cofactor for Rev function,
868 promotes release of HIV RNAs from the perinuclear region. Genes Dev. 2004;18:23-34.
869 20. Zhou Y, Rojas MR, Park M-R, Seo YS, Lucas WJ, Gilbertson RL. Histone H3 interacts and
870 colocalizes with the nuclear shuttle protein and the movement protein of a geminivirus. J Virol.
871 2011;85: 11821-11832.
872 21. McGarry RC, Barron YD, Carvalho MF, Hill JE, Gold D, Cheung E, et al. A novel Arabidopsis
873 acetyltransferase interacts with the geminivirus movement protein NSP. Plant Cell. 2003;15: 1605-
874 1618.
875 22. Carvalho MF, Lazarowitz SG. Interaction of the movement protein NSP and the Arabidopsis
876 acetyltransferase AtNSI is necessary infection and pathogenicity. J Virol. 2004;78: 11161-11171.
877 23. Florentino LH, Santos AA, Fontenelle MR, Pinheiro GL, Zerbini FM, Baracat-Pereira MC, et
878 al. A PERK-Like receptor kinase interacts with the geminivirus nuclear shuttle protein and
879 potentiates viral infection. J Virol. 2006;80: 6648-6656.
880 24. Fontes EPB, Santos AA, Luz DF, Waclawovsky AJ, Chory J. The geminivirus nuclear shuttle
881 protein is a virulence factor that suppresses transmembrane receptor kinase activity. Genes Dev.
882 2004;18: 2545-2556.
883 25. Carvalho CM, Santos AA, Pires SR, Rocha CS, Saraiva DI, Machado JPB, et al. Regulated
884 nuclear trafficking of rpL10A mediated by NIK1 represents a defense strategy of plant cells against
885 virus. PLoS Pathog. 2008c;4: e1000247.
886 26. Zorzatto C, Machado JPB, Lopes KVG, Nascimento KJT, Pereira WA, Brustolini OJB, et al.
887 NIK1-mediated translation suppression functions as a plant antiviral immunity mechanism.
888 Nature. 2015;520: 679-682.

889 27. Sanderfoot AA, Ingham DJ, Lazarowitz SG. A viral movement protein as a nuclear shuttle.
890 The geminivirus BR1 movement protein contains domains essential for interaction with BL1 and
891 nuclear localization. Plant Physiol. 2006;110: 23-33.
892 28. Sanderfoot AA., Lazarowitz SG. Getting it together in plant virus movement: cooperative
893 interactions between bipartite geminivirus movement proteins. Trends Cell Biol. 1996;6: 353-358.
894 29. Ward BM, Medville E, Lazarowitz SG, Turgeon R. The geminivirus BL1 movement protein
895 is associated with endoplasmic reticu- lum-derived tubules in developing phloem cells. J Virol.
896 1997;71: 3726-3733.
897 30. Zhang SC, Wege C, Jeske H. Movement proteins (BC1 and BV1) of Abutilon mosaic
898 geminivirus are cotransported in and between cells of sink but not of source leaves as detected by
899 green fluorescent protein tagging. Virology. 2001;290: 249-260.
900 31. Aberle HJ, Rütz ML, Karayavuz M, Frischmuth S, Wege C, Hülser D, et al. Localizing BC1
901 movement proteins of Abutilon mosaic geminivirus in yeasts by subcellular fractionation and
902 freeze-fracture immunolabelling. Arch Virol. 2002;147:103-107.
903 32. Frischmuth S, Wege C, Hülser D, Jeske H. The movement protein BC1 promotes redirection
904 of the nuclear shuttle protein BV1 of Abutilon mosaic geminivirus to the plasma membrane in
905 fission yeast. Protoplasma. 2007;230:117-123.
906 33. Krenz B, Windeisen V, Wege C, Jeske H, Kleinow T**.** A plastid-targeted heat shock cognate
907 70 kDa protein interacts with the Abutilon mosaic virus movement protein. Virology. 2010;401:6-
908 17.
909 34. Krenz B, Jeske H, Kleinow T. The induction of stromule formation by a plant DNA-virus in
910 epidermal leaf tissues suggests a novel intra- and intercellular macromolecular trafficking route.
911 Front Plant Sci. 2012;3: 291.

912 35. Lewis JD, Lazarowitz SG. *Arabidopsis* synaptotagmin SYTA regulates endocytosis and virus
913 movement protein cell-to-cell transport. Proc Natl Acad Sci, USA. 2010;107: 2491-2496.
914 36. Krapp S, Schuy C, Greiner E, Stephan I, Alberter B, Funk C, et al. Begomoviral movement
915 protein effects in human and plant cells: towards new potential interaction partners. Viruses.
916 2017;9: 334.
917 37. Yazaki J, Galli M, Kim AY, Nito K, Aleman F, Chang KN, et al. Mapping transcription factor
918 interactome networks using HaloTag protein arrays. Proc Natl Acad Sci, USA. 2016;113: e4238-
919 47
920 38. Alcaide-Loridan C, Jupin I. Ubiquitin and plant viruses, let's play together! Plant Physiol.
921 2012;160: 72-82.
922 39. Conchon S, Cao X, Barlowe C, Pelham HR. Got1p and Sft2p: membrane proteins involved in
923 traffic to the Golgi complex. EMBO J. 1999;18: 3934-3946.
924 40. Jung JJ, Inamdar SM, Tiwari A, Choudhury A. Regulation of intracellular membrane
925 trafficking and cell dynamics by syntaxin-6. Biosci Rep. 2012;32: 383-391.
926 41. Drakakaki G, van de Ven W, Pan S, Miao Y, Wang J, Keinath NF, et al. Isolation and proteomic
927 analysis of the SYP61 compartment reveal its role in exocytic trafficking in Arabidopsis. Cell Res.
928 2012;22: 413-424.
929 42. Zhourar J, Rojo E, Bassham DC. AtVPS45 Is a Positive Regulator of the SYP41/SYP61/VTI12
930 SNARE Complex Involved in Trafficking of Vacuolar Cargo. Plant Physiol. 2009;149: 1668-
931 1678.
932 43. Hachez C, Laloux T, Reinhardt H, Cavez D, Degand H, Grefen C, et al. Arabidopsis SNAREs
933 SYP61 and SYP121 coordinate the trafficking of plasma membrane aquaporin PIP2;7 to modulate
934 the cell membrane water permeability. Plant Cell. 2014;26: 3132-3147.

935 44. Reverter M, Rentero C, Garcia-Melero A, Hoque M, Vilà de Muga S, Alvarez-Guaita, A et al.
936 Cholesterol regulates Syntaxin 6 trafficking at trans-Golgi network endosomal boundaries. Cell
937 Rep. 2014;7: 883-97
938

939 45. Robatzek S, Chinchilla D, Boller T. Ligand-induced endocytosis of the pattern recognition
940 receptor FLS2 in Arabidopsis. Genes Dev. 2006;20: 537-542.

941 46. Nelson BK, Cai X, Nebenfuhr A. A multicolored set of in vivo organelle markers for co-
942 localization studies in Arabidopsis and other plants. Plant J. 2007;51: 1126-1136.

943 47. Haupt S, Cowan GH, Ziegler A, Roberts AG, Oparka KL, Torrance L. Two Plant–Viral
944 Movement Proteins Traffic in the Endocytic Recycling Pathway. Plant Cell. 2005;17: 164-181.

945 48. Calil IP, Quadros IPS, Araújo TC, Duarte CEM, Gouveia-Mageste BC, Silva JCF, et al. A
946 WW Domain-Containing Protein Forms Immune Nuclear Bodies against Begomoviruses. Mol
947 Plant. 2018;11: 1449-1465.

948 49. Wang T, Li L, Hong W**.** SNARE proteins in membrane trafficking. Traffic. 2017;18:767-775.

949 50. Zhourar, J., Rojo, E., and Bassham, D.C. (2009). AtVPS45 Is a Positive Regulator of the
950 SYP41/SYP61/VTI12 SNARE Complex Involved in Trafficking of Vacuolar Cargo. Plant
951 Physiol. 149: 1668-1678.

952 51. Jahn R, Scheller RH. SNAREs—Engines for membrane fusion. Nat Rev Mol Cell Biol. 2006;**7**:
953 631-643.

954 51. Edgar RC. MUSCLE: multiple sequence alignment with high accuracy and high throughput.
955 Nucleic Acids Res. 2004;32(5): 1792-1797.

956 52. Ronquist F, Huelsenbeck JP. MrBayes 3: Bayesian phylogenetic inference under mixed
957 models. Bioinformatics. 2003;19: 1572-1574.

958 53. Brandes U. A faster algorithm for betweenness centrality. J Mathem Sociol. 2001;25: 163-177.

54. Freeman LC. Centrality in social networks conceptual clarification. Social Networks. 1978;1: 215-239.

55. Hage P, Harary F. Eccentricity and centrality in networks. Social Networks. 1995;17: 57-63.

56. Falcon S, Gentleman R. Using GOstats to test gene lists for GO term association. Bioinformatics. 2007;23: 257–258.

57. Zhang X, Henriques R, Lin SS, Niu QW, Chua NH. Agrobacterium-mediated transformation of Arabidopsis thaliana using the floral-dip method. Nat Protoc. 2006;1: 641-646.

58. Santos AA, Carvalho CM, Florentino LH, Ramos JJO, Fontes EPB. Conserved threonine residues within the A-loop of the receptor NIK differentially regulate the kinase function required for antiviral signaling. PLoS ONE. 2009;4: e5781.

59. Rocha CS, Santos AA, Machado JPB, Fontes EPB. The ribosomal protein L10/QM-like protein is a component of the NIK-mediated antiviral signaling. Virology. 2008;380: 165–169.

60. Dellaporta SL, Wood J, Hicks JB. 1983. A plant DNA minipreparation: version II. Plant Mol Biol Rep. 1983;1: 19-23.

61. Rojas MR, Gilbertson RL, Russel DR, Maxwell DP. Use of degenerate primers in the polymerase chain reaction to detect whitefly-transmitted geminiviruses. Plant Dis. 1993;77: 340-347.

62. Alves MS, Reis PAB, Dadalto SP, Faria JAQA, Fontes EPB, Fietto LG. A Novel Transcription Factor, ERD15 (Early Responsive to Dehydration 15), Connects Endoplasmic Reticulum Stress with an Osmotic Stress-induced Cell Death Signal. J Biol Chem. 2011;286: 20020-20030.

63. Yamaguchi N, Winter CM, Wu MF, Kwon CS, William DA, Wagner D. Protocols: chromatin immunoprecipitation from Arabidopsis tissues. Arabidopsis Book. 2014;12: e0170.

982 **Figure Legends**

983

984 **Fig 1. MP-NSP-Arabidopsis protein-protein interactions (PPI) network**
985 **integrated into Arabidopsis interactome.**

986 The network displays a firework topology, which was assembled by the Cytoscape software. The
987 viral proteins, MP and NSP, are represented in red. The NSP-specifically interacting proteins are
988 in dark orange and connecting proteins from Arabidopsis in light orange. The MP-specifically
989 interacting proteins are indicated in light yellow to which interacting dark yellow proteins
990 converge. Arabidopsis proteins that interact with both MP and NSP are shown in green, forming
991 hubs of convergent blue proteins. Gray proteins represent connecting points between two
992 functionally similar hubs.

993

994 **Fig 2. NISP, but not AT2G18860, interacts with NSP via the Syntaxin-6 domain.**

995 **(A)** Schematic representation of NISP and AT2G18860 sequence alignment. The syntaxin-6
996 domain is indicated in green and the transmembrane segment, in red. The identity of sequence and
997 positions of amino acid residues are indicated. Sequence alignment was performed with
998 CLUSTAL OMEGA. **(B)** NISP and NSP interact in yeast. NISP and NSP fused to the activation
999 domain (AD), and binding domain (BD) of Gal4 and also in combination with empty vectors were
1000 expressed in yeast. The interactions between the tested proteins were monitored by histidine
1001 prototrophy in medium supplemented with 3-AT for 4 days at 28°C. **(C)** AT2G18860 failed to
1002 interact with NSP in yeast. AT2G18860 and NSP fused to both Gal4AD and BD were expressed
1003 in yeast, and possible interactions were assayed in all combinations. Co-expressed NSP-BD and
1004 NISP-AD were used as a positive control. **(D-F)**. Mapping the NSP-binding domain on NISP.

1005 Yeast cells expressing the indicated truncated version of NISP and NSP fusions were plated on
1006 selective medium lacking leucine, tryptophan, and histidine and supplemented with 2.5 mM 3-AT
1007 and grown for 4 days at 28°C. The truncated versions of NISP are delimited by the indicated
1008 position of the amino acid residues in the full-length protein. Protein interaction was only observed
1009 by co-expressing AD-NISP$^{1-107}$ and BD-NSP.
1010

1011 **Fig 3. Subcellular localization of NISP.**

1012 **(A)** The NISP-GFP distribution in intracellular vesicles. *N. benthamiana* leaves were infiltrated
1013 with *A. tumefaciens* carrying a DNA construct expressing NISP-GFP under the control of 35S
1014 promoter. Confocal images from three independent experiments were taken 36 hours post-
1015 infiltration. Approximately 200 cells were examined. Scale bars, 10 μm and 20 μm. **(B)** Confocal
1016 images of NISP-GFP transiently expressed under the control of the endogenous promoter. Scale
1017 bars, 10 μm and 20 μm. **(C)** Co-expression of the ER-associated ER-mCherry molecular marker
1018 and NISP-GFP in *N. benthamiana* leaves. *N. benthamiana* leaf cells expressing the indicated
1019 fusion proteins were examined by confocal microscopy 2 days after infiltration. The asterisks
1020 indicate the local of the amplified insets, and the arrows indicate the merged pattern of GFP-
1021 associated vesicles in C, D, E, F, G, H. The confocal images are representative samples from three
1022 independent experiments. Scale bars, 10 μm. **(D)** Co-expression of the Golgi-associated G-
1023 mCherry molecular marker and NISP-GFP in *N. benthamiana* leaves 2 days after agro-infiltration.
1024 Scale bars, 20 μm. **(E)** Co-expression of the tonoplast-associated vac-mCherry molecular marker
1025 and NISP-GFP in *N. benthamiana* leaves 2 days after agro-infiltration. Scale bars, 20 μm. **(F)** Co-
1026 expression of the plasma membrane-associated FLS2-mCherry and NISP-GFP in *N. benthamiana*
1027 leaves 2 days after agro-infiltration. Scale bars, 20 μm. **(G)** Co-expression of endosome-associated

1028 SYTA-mCherry and NISP-GFP in *N. benthamiana* leaves 2 days after agro-infiltration. Scale bars,
1029 10 μm. **(H)** Co-labeling of vesicles with NISP-GFP and FM4-64 in epidermal cells of *N.*
1030 *benthamiana.* Images were taken after 2 days post infiltration of *Agrobacterium* carrying a NISP-
1031 GFP expression vector and 1 h after infiltration of FM4-64. Scale bars, 20 μm.
1032

1033 **Fig 4. NISP interacts with NSP *in vivo.***

1034 **(A)** NISP interacts with NSP in vesicle-like compartments, as judged by BiFC. *N. benthamiana*
1035 leaf cells expressing NISP and NSP fused to the C-terminus (cYFP) or N-terminus (nYFP) of YFP,
1036 or in combination with the empty vectors, were observed by confocal microscopy 3 days after
1037 infiltration. Scale bars, 10 μm. The experiment was repeated at least four times with identical
1038 results. **(B)** NISP-NSP complex-containing vesicles are stained by FM4-64. *N. benthamiana* leaves
1039 were agroinfiltrated with nYFP-NISP- and cYFP-NSP-expressing DNA constructs. Images were
1040 taken 2 days post agroinfiltration and 30 min after infiltration of FM4-64. Arrows indicate
1041 examples of vesicle-associated reconstituted fluorescent signals that were co-stained by FM4-64.
1042 Scale bars, 10 μm. The experiment was repeated three times with similar results. **(C)** NISP interacts
1043 with NSP *in planta*. Whole cell protein extracts from N. benthamiana leaves expressing transiently
1044 NISP-GFP and NSP-6HA were used for co-immunoprecipitation assays using an anti-GFP serum.
1045 Input and IP show the levels of the expressed proteins NSP-6HA, NISP-GFP, and GFP. Anti-HA
1046 antibody was used to detect NSP-6HA from the immunoprecipitated complex. GFP was used as a
1047 negative control. Molecular mass markers are given on the left in kilodaltons. The experiment was
1048 repeated twice. **(D)** *In vivo* interaction of NISP with NSP. Co-immunoprecipitation was performed
1049 as described in B, except that the tags of the transiently expressed proteins were switched to NSP-
1050 GFP and NISP-6HA. The experiment was repeated twice.

1051

1052 **Fig 5. NISP displays a pro-begomoviral function.**

1053 **(A)** Transcript accumulation of NISP in transgenic lines. NISP transcript levels in three
1054 independently complemented transgenic lines (*nisp-1*/NISP-1-3), three independently transformed
1055 *NISP*-overexpressing lines (AtNISP1-3), Col-0 and *nisp-1* were determined by qRT-PCR. Gene
1056 expression was calculated using the $2^{-\Delta Ct}$ method, and actin was used as an endogenous control.
1057 Error bars represent 95% confidence intervals based on replicated samples (n=3) from three
1058 independent experiments. **(B)** NISP-GFP protein accumulation in transgenic lines. Whole cell
1059 protein extracts from the complemented transgenic lines (*nisp-1*/NISP), *NISP*-overexpressing lines
1060 (AtNISP), Col-0 and *nisp-1* were separated by SDS-PAGE and immunoblotted using an anti-GFP
1061 serum. **(C)** AT2G18860 transcript accumulation in transgenic lines. The transcript levels of
1062 AT2G18860 in complemented transgenic lines (*at2g18860-1*/AT2G18860-1-3), AT2G18860-
1063 overexpressing lines (AT2G18860-1-3), Col-0 and *at2g18860-1* were quantified by qRT-PCR and
1064 normalized to the actin as an endogenous control. Error bars indicate 95% confidence intervals
1065 based on replicated samples (n=3) from three independent experiments. **(D)** AT2G18860-GFP
1066 protein accumulation in transgenic lines. Total protein extracts from complemented transgenic
1067 lines (*at2g18860-1*/AT2G18860), AT2G18860-overexpressing lines (AT2G18860), Col-0 and
1068 *at2g18860-1* were fractionated by SDS-PAGE and immunoblotted using anti-GFP antibody. **(E)**
1069 CaLCuV infection-associated symptoms in Arabidopsis genotypes at 21 days post-inoculation
1070 (dpi). The figure shows representative samples of mock-inoculated and CaLCuV -infected plants.
1071 The genotypes are indicated in the figure and are the same as specified in A-D. **(F)** The onset of
1072 infection is delayed in *nisp-1* knockout line. Ecotype Col-0, *nisp-1*, *at2g18860-1*, *nisp-1*/NISP
1073 complemented lines and AtNISP-overexpressing lines (as in a-d) were infected with CaLCuV

1074 DNA, and the course of infection was monitored as the percent of systemically infected plants at
1075 different dpi. **(G)** Absolute quantification of CaLCuV genomic units in infected lines at 21 dpi.
1076 The genotypes are the same as specified in a-d. Error bars indicate 95% confidence intervals based
1077 on replicated samples from three independent experiments. Different letters indicate significative
1078 differences among the groups (Duncan test, p <0,05, n= 3).
1079

1080 **Fig 6. NISP interacts with NIG *in vivo* and NSP enhances NISP-NIG complex**
1081 **formation.**

1082 **(A)** BIFC assay showing the interaction between NISP and NIG in vesicles of *N. benthamiana* leaf
1083 cells. *N. benthamiana* leaves transiently expressing NISP and NIG fused to the C-terminus (cYFP)
1084 or N-terminus (nYFP) of YFP were examined by confocal microscopy 3 days after infiltration.
1085 Scale bars, 10 µm and 20 µm. The experiment was repeated three times with similar results. **(B)**
1086 NISP-NIG complex-containing vesicles are stained by FM4-64. *N. benthamiana* leaves were
1087 agroinfiltrated with nYFP-NIG- and cYFP-NISP-expressing DNA constructs. Images were taken
1088 2 days post infiltration and 1 h after infiltration of FM4-64. Arrows indicate examples of vesicle-
1089 associated reconstituted fluorescent signals that were co-stained by FM4-64 and the asterisk, the
1090 region of the amplified inset. Scale bars, 10 µm. The experiment was repeated three times with
1091 identical results. **(C)** In vivo interaction of NISP and NIG. Total protein extracts from *N.*
1092 *benthamiana* expressing NISP-GFP and NIG-6HA were used for co-immunoprecipitation assays
1093 using anti-GFP. Input and IP show the levels of the expressed proteins NISP-GFP and NIG-6HA.
1094 Anti-HA was used to detect NIG-6HA from the immunoprecipitated complex. GFP was used as
1095 an unrelated protein. The experiment was repeated twice with identical results. **(D)** NISP-NIG
1096 complex formation in the presence of viral NSP. The Co-IP assay was performed as described in

1097 A, except that co-expressed NSP-GST was included in the assay. NSP-GST was detected by
1098 immunoprecipitating it from infiltrated leaves and immunoblotting with anti-GST. The experiment
1099 was repeated twice with identical results. **(E)** Viral NSP enhances the interaction between NISP
1100 and NIG. NIG levels in the immunoprecipitated complex in the presence and absence of viral NSP
1101 were quantified using the Band Analysis tools of the ImageLab software (Bio-Rad). The signal
1102 values were normalized using the IP NISP-GFP band. A.U. denotes arbitrary units.
1103

1104 **Fig 7. NISP complexes with vDNA *in vivo.***

1105 **(A)** NISP-GFP accumulation in overexpressing lines. Whole cell protein extracts from the NISP-
1106 GFP-overexpressing lines, as indicated in the figure, and Col-0 were separated by SDS-PAGE and
1107 immunoblotted using an anti-GFP serum. **(B)** NISP binds to viral DNA-B *in vivo*. NISP-GFP-
1108 overexpressing lines (AtNISP-1, AtNISP-2, and AtNISP-3), and Col-0 were inoculated with
1109 infectious CaLCuV clones prior to the ChIP assay, which was performed with leaf samples of the
1110 indicated genotypes using anti-GFP. The infected plants were confirmed by PCR of input DNA
1111 from inoculated plants using CaLCuV DNA-B-specific primers, which amplifies a 770-bp
1112 fragment (F1/R1; S10b Fig). IN denotes infected leaves and UN, uninfected leaves. **(C)** ChIP-
1113 qPCR assay of leaves from AtNISP-GFP transgenic lines and Col-0. The samples were
1114 immunoprecipitated with an anti-GFP antibody and ChIPed DNA was quantified by qPCR using
1115 the DNA-B-specific primers F3/R3 (S10b Fig). Data were normalized relative to the input of each
1116 sample and are expressed as the percentage of input. (D) ChIP-qPCR assay using a different set of
1117 DNA-B-specific primers (F2/R2) and samples from the indicated genotypes. The ChIP-qPCR was
1118 performed as described in C. **(E)** NISP binds to viral DNA-A *in vivo*. NISP-GFP-overexpressing
1119 lines (AtNISP-1, AtNISP-2 and AtNISP-3), and Col-0 were inoculated with infectious CaLCuV

1120 clones prior to the ChIP assay, which was performed with leaf samples of the indicated genotypes
1121 using anti-GFP. The infected plants were confirmed by PCR of input DNA from inoculated plants
1122 using CaLCuV DNA-A-specific primers, which amplifies a 389-bp fragment (F1/R1; S10a Fig).
1123 IN denotes infected leaves and UN, uninfected leaves. **(F)** ChIP-qPCR assay using a set of DNA-
1124 A-specific primers (F2/R2, S10a Fig) and samples from the indicated genotypes. The ChIP-qPCR
1125 was performed as described in C. The above experiments were repeated three times with similar
1126 results.
1127

1128 **Supporting information**

1129 **S1 Table-** Protein-protein interactions between the viral proteins and the
1130 Arabidopsis proteins**.**
1131

1132 **S2 Table-** Enriched GO terms in three categories, Biological Process, Molecular
1133 Function, or Cellular Component ontology
1134

1135 **S3 Table.** List of primers used for cloning, PCR, RT-qPCR and qPCR
1136

1137 **S4 Table.** Expression of kanamycin resistance in the T1 generation of transgenic
1138 Arabidopsis plants.
1139

1140 **S1 Video/Movie** -Vesicle-associated localization of NISP

1141 **S1 Fig. Identification of MP- and NSP-interacting proteins.**

1142 **(A)** *In vitro* synthesized 3xHA-NSP and 3xHA-MP. In vitro translated HA-NSP and HA-MP were
1143 electrophoresed by SDS-PAGE and immunoblotted using an anti-HA antibody. **(B)** Protein
1144 interaction between *in situ* synthesized Arabidopsis hallo-proteins and 3xHA-MP or 3xHA-NSP.
1145 The AtNAPPA02 high-density array containing 4600 Arabidopsis ORFS spotted in duplicates was
1146 probed with 3xHA-MP or 3xHA-NSP, and candidate interactors were detected with an anti-HA
1147 antibody. The bright spots are signals from candidate interactors.

1148 **S2 Fig. A network of NSP- and MP-directly interacting Arabidopsis proteins.**

1149 The network was assembled by the Cytoscape software. The viral proteins are indicated in red,
1150 MP-specifically interacting proteins in yellow, NSP-specifically interacting proteins in orange and
1151 proteins that associate with both MP and NSP are indicated in green.

1152

1153 **S3 Fig. *In silico* analyses of NISP.**

1154 **(A)** Phylogenetic tree of syntaxin superfamily domain-containing proteins from the species
1155 indicated. The phylogenetic tree was constructed using Bayesian inference performed with
1156 MrBayes v3.2.2 and the mixed amino acid substitution model Wag. The syntaxin-6 domain-
1157 containing proteins from Arabidopsis are indicated in blue, and NISP (AT4G30240) was clustered
1158 with plant-specific syntaxin-6 proteins forming the red clade. **(B)** Phylogenetic tree of N-terminal
1159 Syntaxin-6 domain-containing proteins. NISP (AT4G30240) clusters together with plant-specific
1160 N-terminal syntaxin-6 proteins, which do not harbor a typical tSnare domain at the C-terminus.
1161 The syntaxin-6 domain proteins from Arabidopsis are in blue. The phylogenetic tree was
1162 constructed using Bayesian inference performed with MrBayes v3.2.2 and the mixed amino acid
1163 substitution model Jones.

1164

1165 **S4 Fig. Sequence alignment of NSP and AT2G18860**

1166 The N-terminal syntaxin-6 domain is indicated in red and the transmembrane segment in black.
1167 The sequence alignment was performed using CLUSTAL OMEGA. Identical amino acids are
1168 indicated with asterisks, highly conserved residues with (:) and lower conservation with (.).

1169

1170 **S5 Fig. Subcellular localization of AT2G18860**

1171 AT2G18860-GFP distribution in plasma membrane-associated vesicles. *N. benthamiana* leaves
1172 were infiltrated with *A. tumefaciens* carrying a DNA construct expressing AT2G18860-GFP under
1173 the control of 35S promoter. Confocal images were taken 36 h post-infiltration. Approximately
1174 200 cells were examined. Scale bars, 10 μm.

1175

1176 **S6 Fig**. ***NISP*, but not AT2G18860, expression is induced by CaLCuV**

1177 NISP and AT2G18860 transcript levels were quantified by qRT-PCR in uninfected Col-0 leaves
1178 (Col-0), tungsten-inoculated Col-0 leaves (Col-0 T), and systemically infected Col-0 leaves with
1179 CaLCuV (Col-0 IN). Gene expression was calculated using the $2^{-\Delta Ct}$ method, and actin was used
1180 as an endogenous control. Error bars indicate 95% confidence intervals based on replicated
1181 samples (n = 3) from three independent experiments.

1182

1183 **S7 Fig. The transgenic lines are visibly indistinguishable from the wild-type plants.**

1184 Columbia (Col-0) ecotype of *Arabidopsis thaliana* was used as the wild-type control for phenotype
1185 comparison, and the Col-0 ecotype was used for generating almost all the transgenic plants except
1186 for the complementation test in *nik1-1* and *at2g18860-1* mutants. The genotypes are the same as

1187 in Fig. 5. Plants were grown in a growth chamber at 22°C under long-day conditions (16 h light/8
1188 h dark). **(A)** Developmental phenotypes associated with inactivation of NISP gene and
1189 overexpression of NISP-GFP in the R3 generation of transgenic lines at 45 days after germination.
1190 **(B)** Developmental phenotypes associated with inactivation of NISP gene and overexpression of
1191 NISP-GFP in the R3 generation of transgenic lines at 60 days after germination. **(C)**
1192 Developmental phenotypes associated with inactivation of AT2G18860 gene and overexpression
1193 of AT2G18860-GFP in the R2 generation of transgenic lines at 45 days after germination. **(D)**
1194 Developmental phenotypes associated with inactivation of AT2G18860 gene and overexpression
1195 of AT2G18860-GFP in the R2 generation of transgenic lines at 60 days after germination
1196

1197 **S8 Fig 8. NSP enhances NISP-NIG complex formation.**

1198 **(A)** NISP interacts with NIG in yeast. AD-NIG and BD-NISP fusions were expressed in yeast and
1199 interactions between the recombinant proteins were monitored by His prototrophy in selective
1200 medium (-Leu,-Trp,-His) and supplemented with 2.5 mM 3-AT. The co-expression of PRNIG
1201 fused to BD and CSN5A fused to AD was used as a positive control. **(B)** Cytosolic and perinuclear
1202 distribution of NIG-GFP. *N. benthamiana* leaves were infiltrated with A. tumefaciens carrying
1203 NIG-GFP constructs with expression driven by the 35S constitutive promoter. NIG-GFP was
1204 imaged by confocal microscopy 36 h after infiltration. **(C)** Cytosolic localization of NIG in
1205 transgenic lines. Confocal fluorescence image of Arabidopsis root cells stably transformed with
1206 35S:NIG-GFP. **(D)** NISP interacts with NIG *in planta*. Total protein extracts from *N. benthamiana*
1207 expressing NISP-6HA and NIG-GFP were used for co-immunoprecipitation assays using anti-
1208 GFP. Input and IP show the levels of the expressed proteins NISP-6HA and NIG-GFP. Anti-HA
1209 was used to detect NISP-6HA from the immunoprecipitated complex. GFP was used as an

1210 unrelated protein. The experiment was repeated three times. **(E)** NISP-NIG complex formation in
1211 the presence of viral NSP. The Co-IP assay was performed as described in A, except that co-
1212 expressed NSP-GST was included in the assay. NSP-GST was detected by immunoprecipitating
1213 it from transfected leaves and immunoblotting with anti-GST. The experiment was repeated three
1214 times. **(F)** The interaction of NISP and NIG is increased by the presence of viral NSP. NIG-GFP
1215 levels in the immunoprecipitated complex in the presence and absence of viral NSP were
1216 quantified using the Band Analysis tools of the ImageLab software (Bio-Rad). The signal values
1217 were normalized using the IP NIG-GFP band. A.U. denotes arbitrary unit.

1218

1219 **S9 Fig. NISP interacts with NIG *in vivo* and NSP enhances NISP-NIG complex formation.**
1220 **(A)** BIFC assay showing the interaction between NISP and NIG in vesicles of *N. benthamiana* leaf
1221 cells. *N. benthamiana* leaves transiently expressing NISP and NIG fused to the C-terminus (cYFP)
1222 or N-terminus (nYFP) of YFP, were examined by confocal microscopy 3 days after infiltration.
1223 Scale bars, 10 μm and 20 μm. **(B)** Co-expression of NSP-6HA strengthens interaction between
1224 NIG and NISP. The BiFC assay was performed by agro-infiltration of *N. benthamiana* leaves with
1225 nYFP-NIG, cYFP-NISP and vice-versus along with the expression of NSP-6HA. The reconstituted
1226 fluorescence signal was observed by confocal microscopy, 3 days after agroinfiltration. The figure
1227 displays representative samples from three independent biological repeats. Scale bars, 10 μm. **(C)**
1228 Confocal fluorescent image of NISP and NIG fused to the C-terminus (cYFP) or N-terminus
1229 (nYFP) of YFP in combination with empty vectors, as indicated in the figure.

1230 **S10 Fig. Schematic representation of CaLCuV DNA-A, DNA-B and ChIP-DNA primers.**
1231 **(A)** Schematic representation of DNA-A. The number 1 corresponds to the 5' end of the nick site
1232 (TAATATT/AC) within the conserved nonanucleotide sequence located in the intergenic region.

1233 The ORFs are indicated with arrows. The positions of the primers used for PCR (F1/R1), and qRT-
1234 PCR (F2/R2) are indicated. **(B)** Schematic representation of DNA-B. The numbering scheme is
1235 the same as in a. The ORFs are indicated with arrows. The positions of the primers used for PCR
1236 (F1/R1), and qRT-PCR (F2/R2 and F3/R3) are indicated.
1237

1238

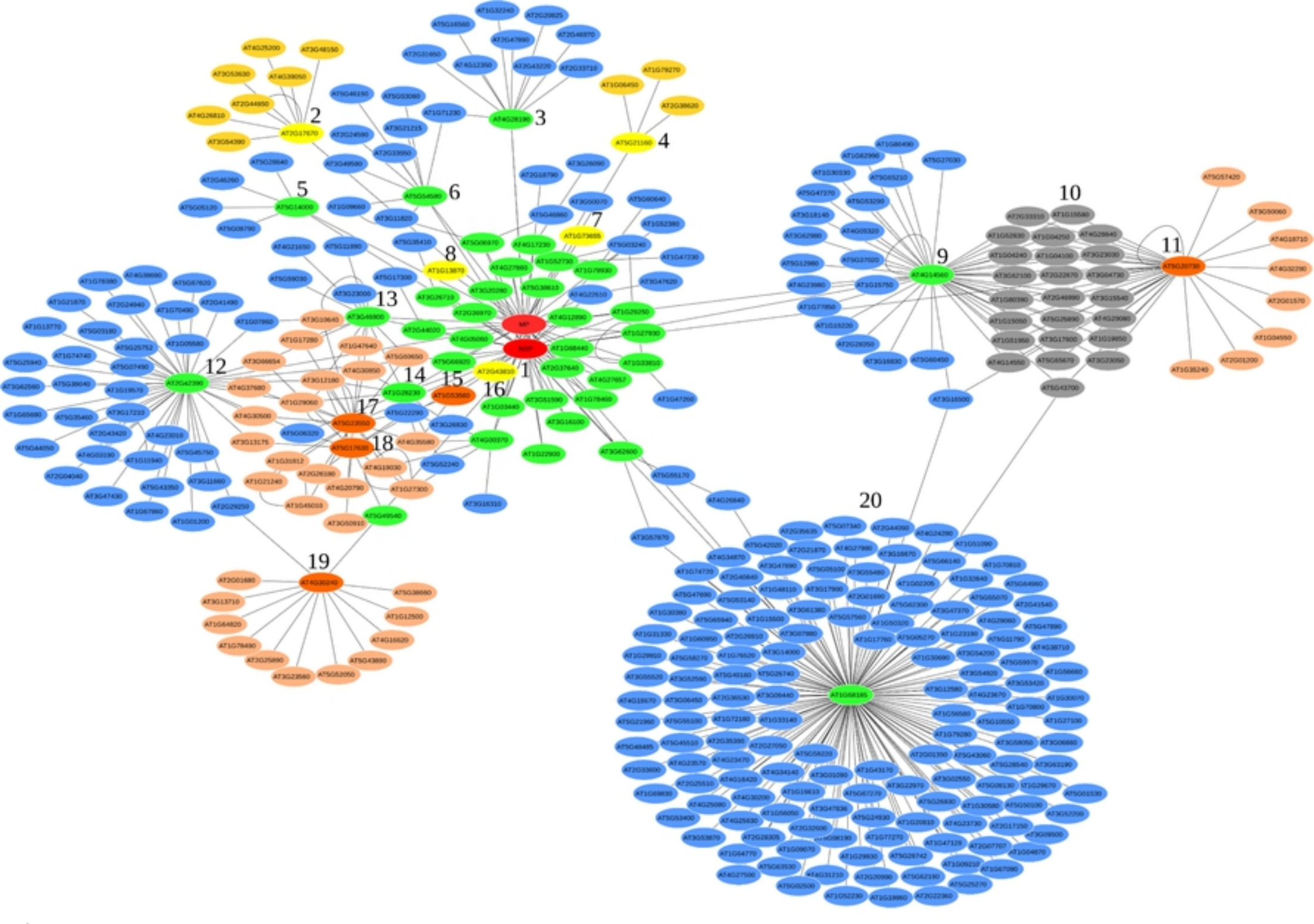

Figure 1

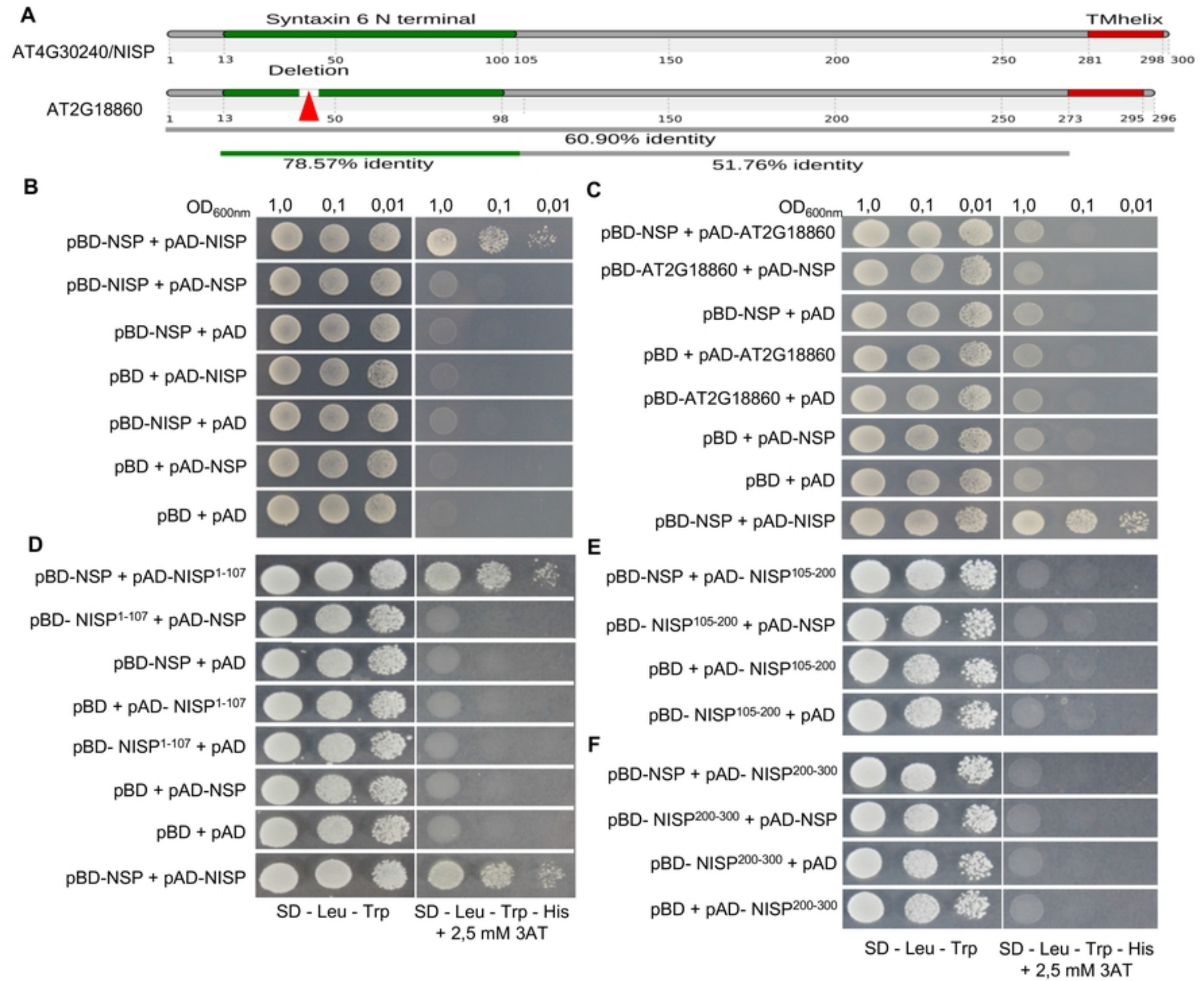
A
Syntaxin 6 N terminal
TMhelix
AT4G30240/NISP
1 13 50 100 105 150 200 250 281 298 300
Deletion
AT2G18860
1 13 50 98 150 200 250 273 295 296
60.90% identity
78.57% identity
51.76% identity
B
OD600nm 1,0 0,1 0,01 1,0 0,1 0,01
pBD-NSP + pAD-NISP
pBD-NISP + pAD-NSP
pBD-NSP + pAD
pBD + pAD-NISP
pBD-NISP + pAD
pBD + pAD-NSP
pBD + pAD
C
OD600nm 1,0 0,1 0,01 1,0 0,1 0,01
pBD-NSP + pAD-AT2G18860
pBD-AT2G18860 + pAD-NSP
pBD-NSP + pAD
pBD + pAD-AT2G18860
pBD-AT2G18860 + pAD
pBD + pAD-NSP
pBD + pAD
pBD-NSP + pAD-NISP
D
pBD-NSP + pAD-NISP1-107
pBD- NISP1-107 + pAD-NSP
pBD-NSP + pAD
pBD + pAD- NISP1-107
pBD- NISP1-107 + pAD
pBD + pAD-NSP
pBD + pAD
pBD-NSP + pAD-NISP
SD - Leu - Trp
SD - Leu - Trp - His + 2,5 mM 3AT
E
pBD-NSP + pAD- NISP105-200
pBD- NISP105-200 + pAD-NSP
pBD + pAD- NISP105-200
pBD- NISP105-200 + pAD
F
pBD-NSP + pAD- NISP200-300
pBD- NISP200-300 + pAD-NSP
pBD- NISP200-300 + pAD
pBD + pAD- NISP200-300
SD - Leu - Trp
SD - Leu - Trp - His + 2,5 mM 3AT

Figure 2

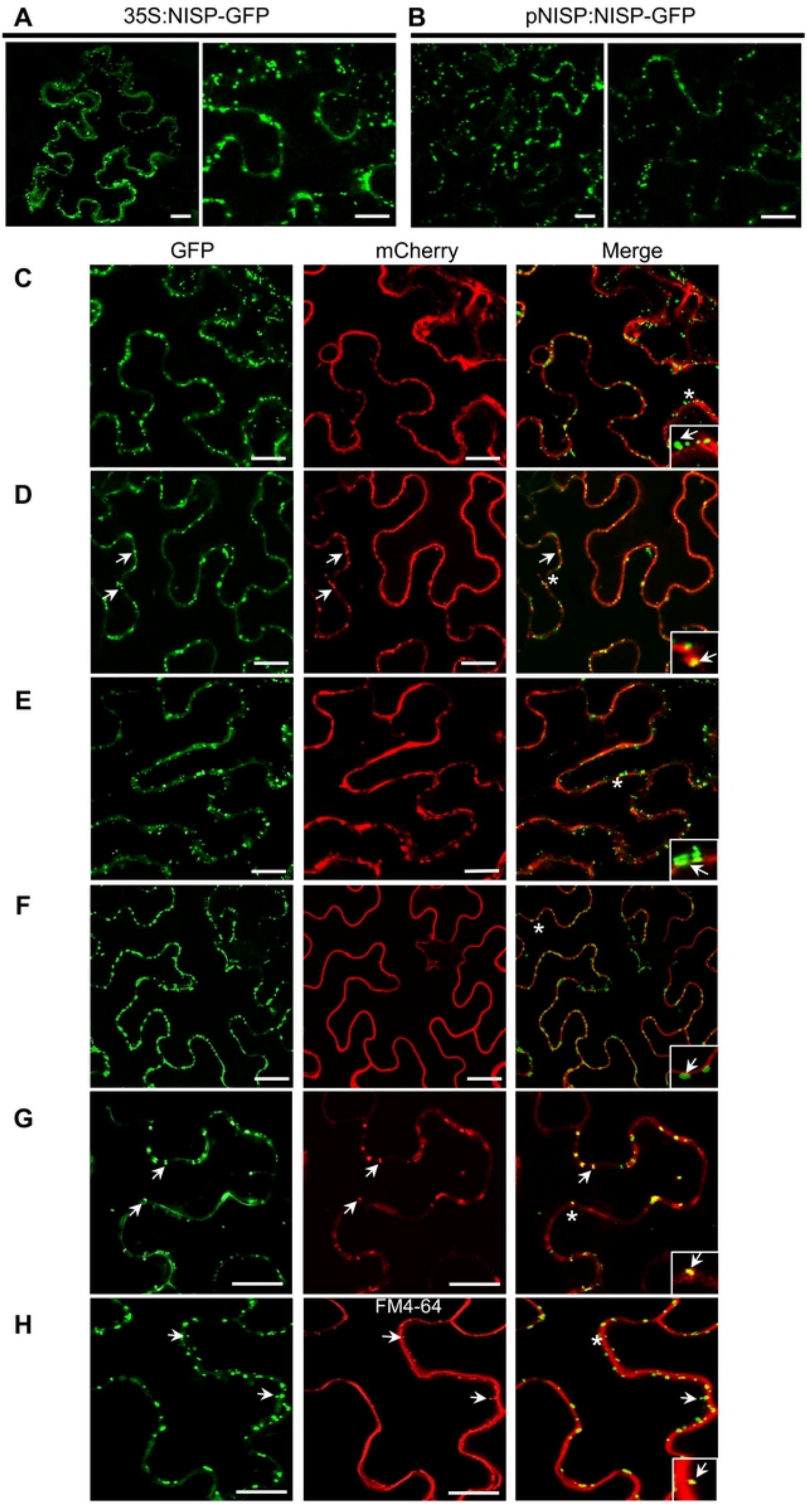
A
35S:NISP-GFP
B
pNISP:NISP-GFP
GFP
mCherry
Merge
C
D
E
F
G
H
FM4-64

Figure 3

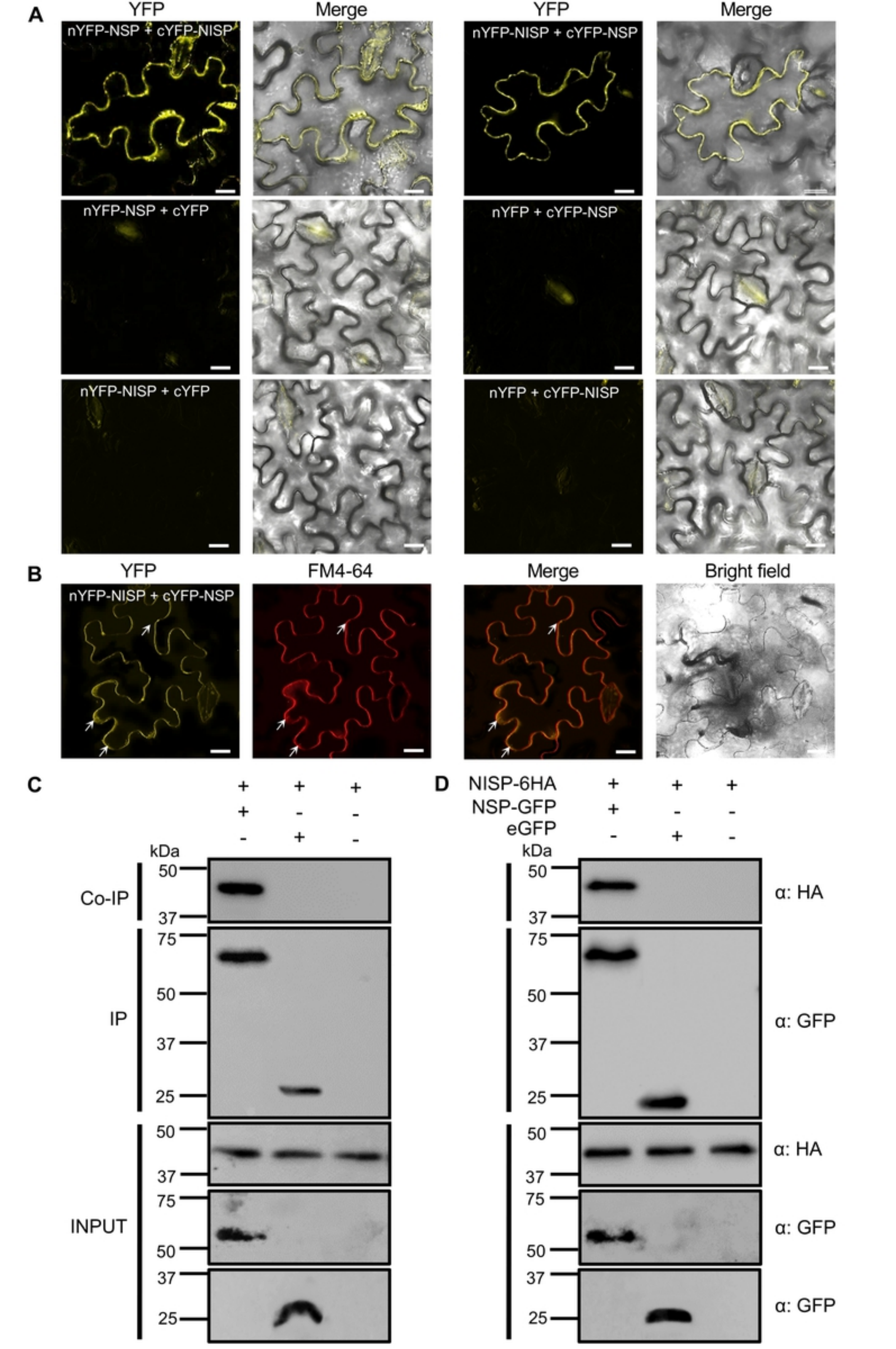
A
YFP
Merge
YFP
Merge
nYFP-NSP + cYFP-NISP
nYFP-NISP + cYFP-NSP
nYFP-NSP + cYFP
nYFP + cYFP-NSP
nYFP-NISP + cYFP
nYFP + cYFP-NISP
B
YFP
FM4-64
Merge
Bright field
nYFP-NISP + cYFP-NSP
C
kDa
Co-IP
IP
INPUT
50
37
75
25
D
NISP-6HA
NSP-GFP
eGFP
α: HA
α: GFP

Figure 4

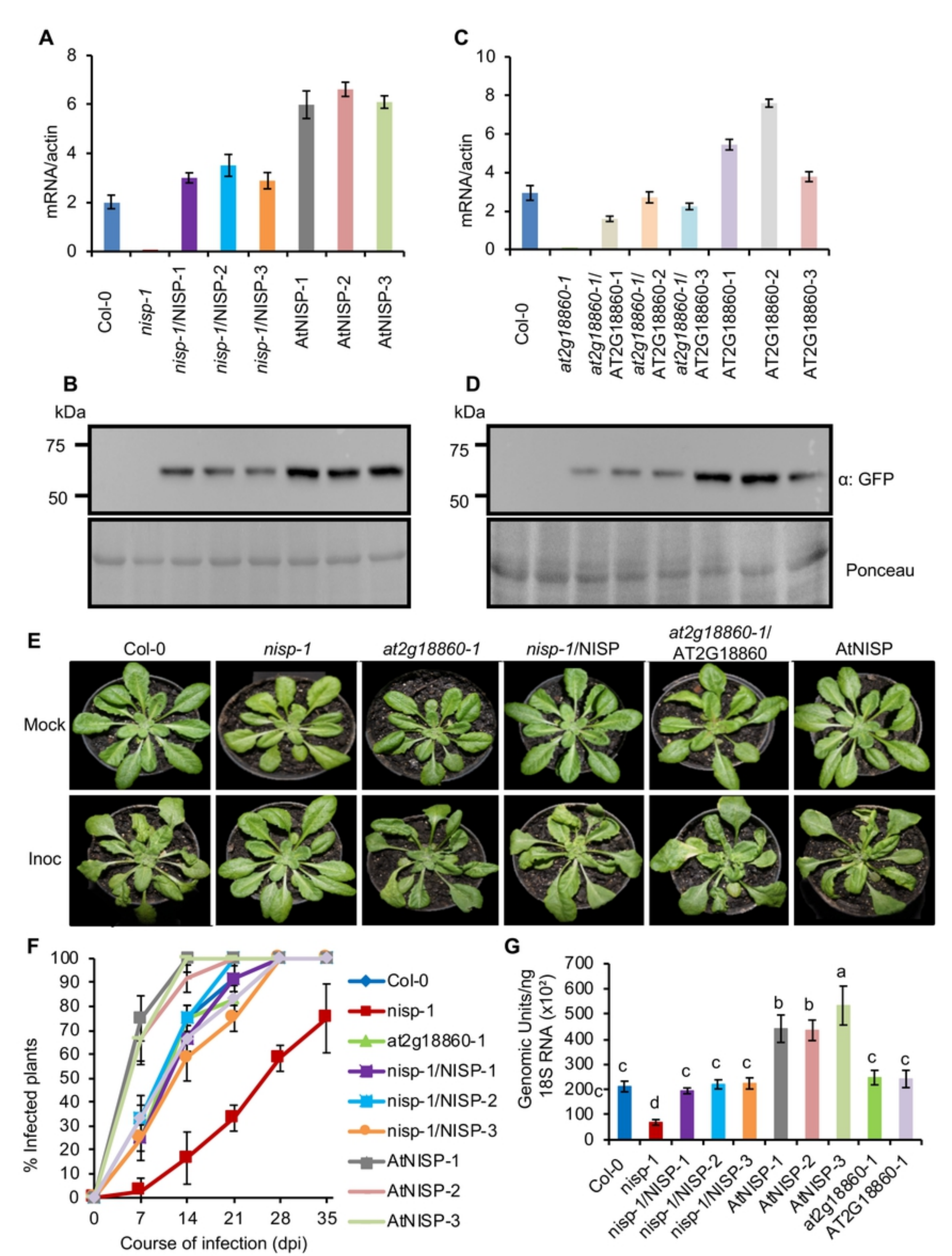
A
mRNA/actin
Col-0
nisp-1
nisp-1/NISP-1
nisp-1/NISP-2
nisp-1/NISP-3
AtNISP-1
AtNISP-2
AtNISP-3
C
mRNA/actin
Col-0
at2g18860-1
at2g18860-1/ AT2G18860-1
at2g18860-1/ AT2G18860-2
at2g18860-1/ AT2G18860-3
AT2G18860-1
AT2G18860-2
AT2G18860-3
B
kDa
75
50
D
kDa
75
50
α: GFP
Ponceau
E
Col-0
nisp-1
at2g18860-1
nisp-1/NISP
at2g18860-1/ AT2G18860
AtNISP
Mock
Inoc
F
% Infected plants
Course of infection (dpi)
Col-0
nisp-1
at2g18860-1
nisp-1/NISP-1
nisp-1/NISP-2
nisp-1/NISP-3
AtNISP-1
AtNISP-2
AtNISP-3
G
Genomic Units/ng 18S RNA (x10²)
Col-0
nisp-1
nisp-1/NISP-1
nisp-1/NISP-2
nisp-1/NISP-3
AtNISP-1
AtNISP-2
AtNISP-3
at2g18860-1
AT2G18860-1

Figure 5

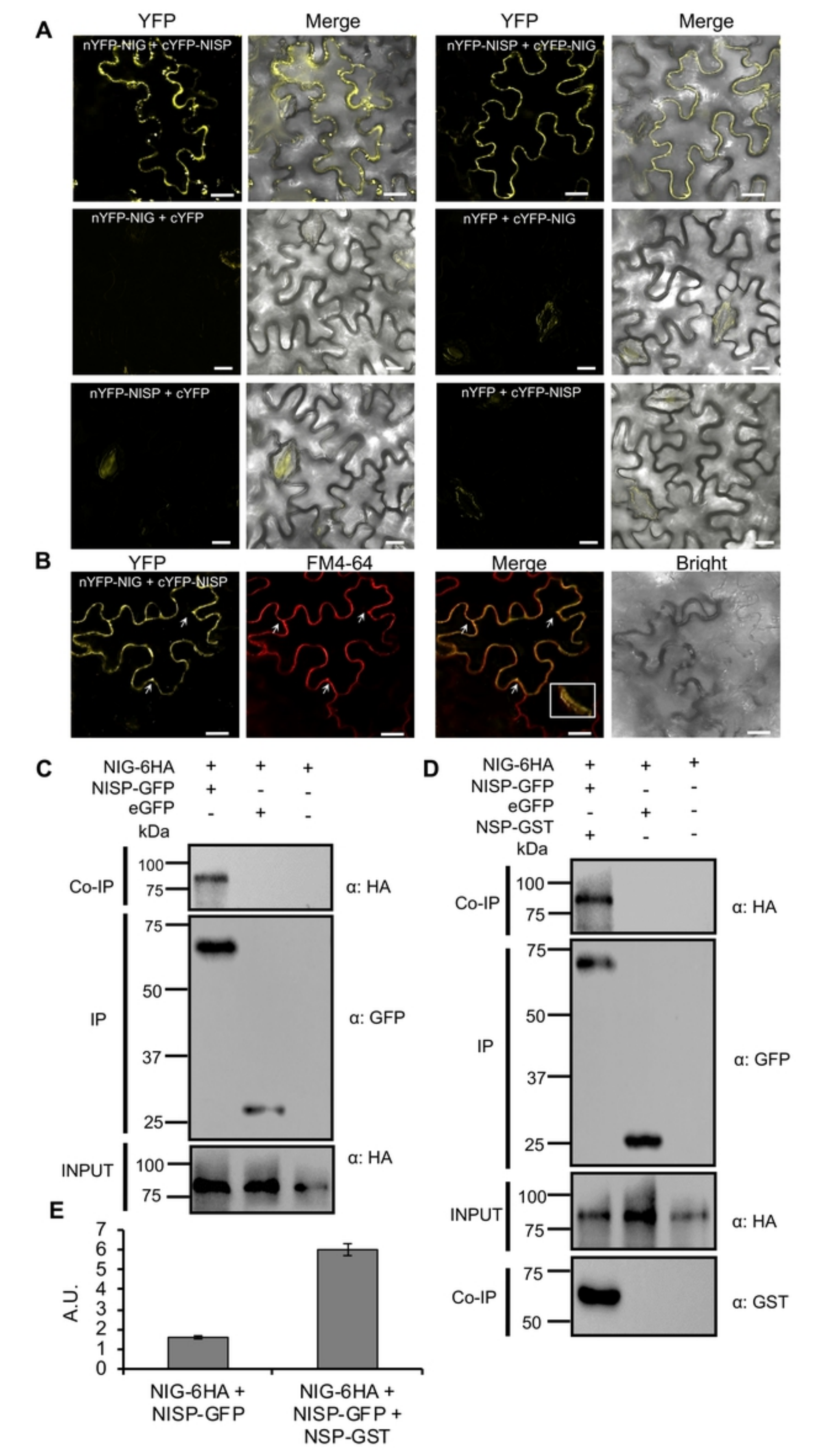
A
YFP
Merge
YFP
Merge
nYFP-NIG + cYFP-NISP
nYFP-NISP + cYFP-NIG
nYFP-NIG + cYFP
nYFP + cYFP-NIG
nYFP-NISP + cYFP
nYFP + cYFP-NISP
B
YFP
FM4-64
Merge
Bright
nYFP-NIG + cYFP-NISP
C
NIG-6HA + + +
NISP-GFP + - -
eGFP - + -
kDa
Co-IP
100
75
α: HA
IP
75
50
37
25
α: GFP
INPUT
100
75
α: HA
D
NIG-6HA + + +
NISP-GFP + - -
eGFP - + -
NSP-GST + - -
kDa
Co-IP
100
75
α: HA
IP
75
50
37
25
α: GFP
INPUT
100
75
α: HA
Co-IP
75
50
α: GST
E
A.U.
7
6
5
4
3
2
1
0
NIG-6HA + NISP-GFP
NIG-6HA + NISP-GFP + NSP-GST

Figure 6

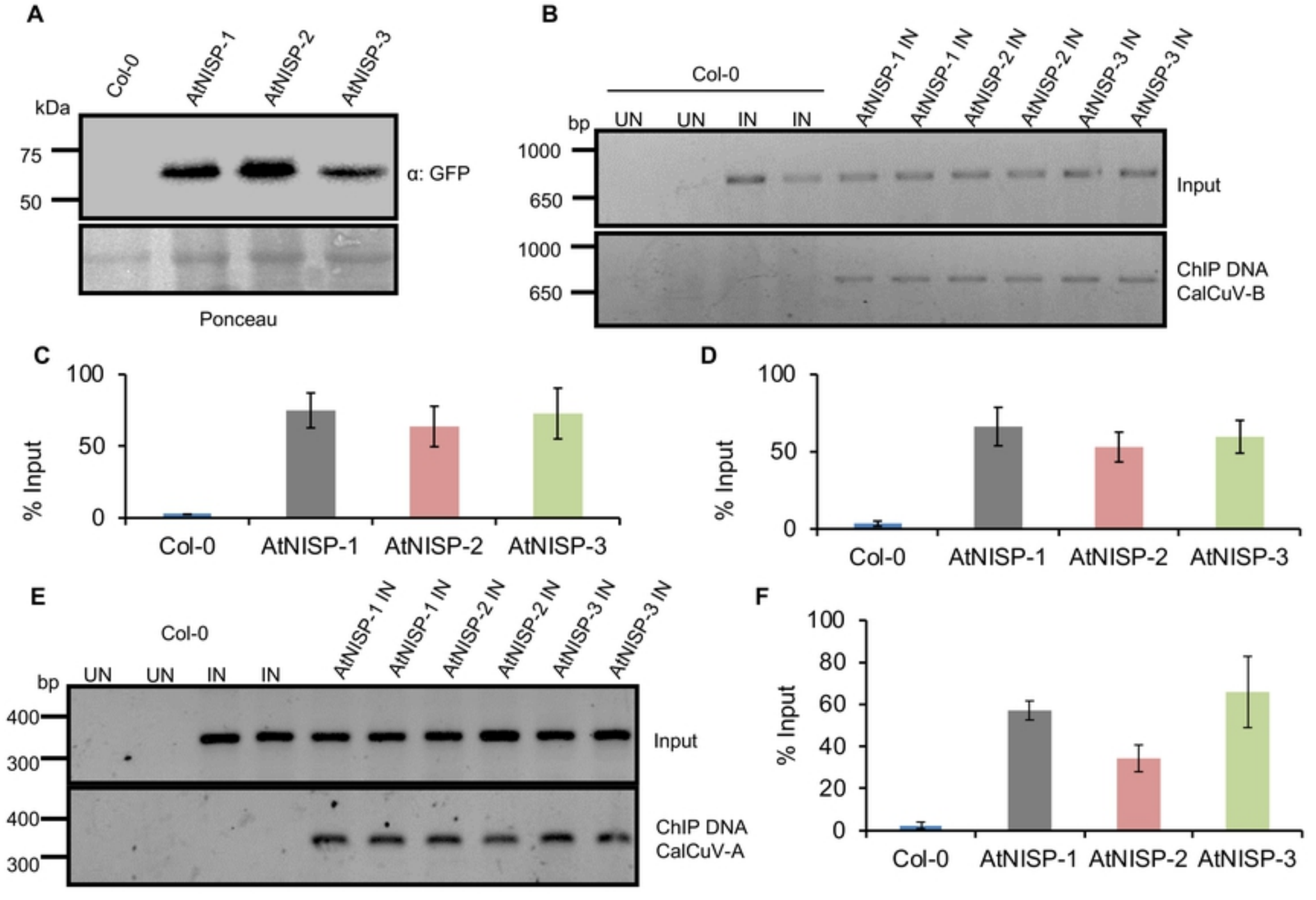
A
Col-0
AtNISP-1
AtNISP-2
AtNISP-3
kDa
75
50
α: GFP
Ponceau
B
Col-0
UN
UN
IN
IN
AtNISP-1 IN
AtNISP-1 IN
AtNISP-2 IN
AtNISP-2 IN
AtNISP-3 IN
AtNISP-3 IN
bp
1000
650
Input
ChIP DNA
CalCuV-B
C
% Input
100
50
0
Col-0
AtNISP-1
AtNISP-2
AtNISP-3
D
% Input
100
50
0
Col-0
AtNISP-1
AtNISP-2
AtNISP-3
E
Col-0
UN
UN
IN
IN
AtNISP-1 IN
AtNISP-1 IN
AtNISP-2 IN
AtNISP-2 IN
AtNISP-3 IN
AtNISP-3 IN
bp
400
300
Input
ChIP DNA
CalCuV-A
F
% Input
100
80
60
40
20
0
Col-0
AtNISP-1
AtNISP-2
AtNISP-3

Figure 7